# Droplet collisions of water and milk in a spray with Langevin turbulence dispersion

Finotello, Giulia; Padding, Johan T.; Buist, Kay A.; Jongsma, Alfred; Innings, Fredrik; Kuipers, J. A.M.

**DOI**
10.1016/j.ijmultiphaseflow.2019.03.003

**Publication date**
2019

**Document Version**
Accepted author manuscript

**Published in**
International Journal of Multiphase Flow

# Droplet collisions of water and milk in a spray with Langevin turbulence dispersion

Giulia Finotello[a], Johan T. Padding[b], Kay A. Buist[a], Alfred Jongsma[c], Fredrik Innings[c], J.A.M. Kuipers[a]

[a] *Multiphase Reactors Group, Department of Chemical Engineering and Chemistry, Eindhoven University of Technology, The Netherlands.*
[b] *Intensified Reaction and Separation Systems, Department of Process and Energy, Delft University of Technology, The Netherlands.*
[c] *Tetra Pak CPS, Heerenveen, The Netherlands.*

**Abstract**

In this work we investigate droplet-droplet collision interactions in a spray system using an Eulerian-Lagrangian model with subgrid turbulence dispersion. The effect of different droplet viscosities on the type and frequency of droplet collision is investigated, knowledge of which is essential for industrial processes such as spray drying for production of milk powder. The dispersed phase is treated with Lagrangian transport of droplets and the turbulent self-induced gas flow using large eddy simulation (LES). A stochastic Direct Simulation Monte Carlo (DSMC) method is used to detect collisions between droplets. The outcome of a binary collision is described by a collision boundary models for water and milk concentrates. A turbulence dispersion model, based on the Langevin equation, accounts for the stochastic subgrid fluid velocity fluctuations along the droplet trajectory. We compare the spray dynamics with and without droplet interactions and turbulence dispersion. For a spray with typical droplet size of 50 $\mu$m, we find that the turbulence dispersion model enhances the total collision frequencies by approximately 25%. The performance of the turbulent dispersion model is tested by investigating the rate of collisions for different milk concentrates. The evolution of size distributions inside the spray is strongly influenced by the complementary effects of collision boundary models and turbulence dispersion.

*Keywords:* Eulerian-Lagrangian model, coalescence, separation, bouncing, Langevin subgridscale model

## 1. Introduction

Atomization of liquids is an important unit operation in industrial and technical processes such as fuel combustion, spray drying, agricultural spraying, paint spraying and air conditioning. For each specific application the atomization process needs to be optimized. Unless the spray is extremely dilute, collision

*Corresponding author
*Email address:* G.Finotello@tue.nl (Giulia Finotello)

and break-up phenomena lead to an evolution of the droplet size distribution along the spray. For rational design of a spray processes, a fundamental understanding of their multiphase flow dynamics is essential.

The most relevant processes to be modelled in a spray are gas flow turbulence, droplet transport and its interaction with the turbulent gas flow and droplet-droplet collisions. In the field of liquid sprays, size and velocity distributions are commonly used to compute parameters that characterize the spray such as the mean velocity and the Sauter Mean Diameter (SMD). Also other properties, describing the droplet interactions, are important to obtain insight into the spray flow. Gavaises et al. [1] evaluated the effect of droplet collisions on the spray mixing of two water nozzles in a cross-flowing gas. They showed that droplet interactions need to be included in order to obtain a good prediction of the spray behaviour.

The dispersion of droplets in a spray depends both on gas parameters, such as velocity, level of turbulence, temperature and pressure, and on the droplet interactions. The coupling between the phases and the prediction of fluctuating velocities have a pronounced influence on the dispersed flow field and on droplet collision probabilities. O'Rourke [2] demonstrated the importance of applying a turbulent dispersion model and the possible errors on particle positions arising by ignoring turbulent contributions.

In our work the droplet drying and heat and mass transfer with the gas phase are not considered. The study of Ruger et al. [3] revealed that the frequently observed changes of the integral droplet Sauter mean diameter along the spray are due mainly to coalescence and break-up instead of droplet evaporation.

Mostafa and Mongia [4] have shown that both Eulerian and the Lagrangian approaches are able to predict the main features of the turbulent dispersion of droplets in a spray. In the Eulerian formulation all the droplets present in the system must be divided into a number of separate size classes, each one requiring its own set of transport equations describing collisions and evaporation. The Lagrangian method has fewer transport equations to solve numerically, but a three-dimensional transient solution is needed to model the effect of collisions and turbulence interactions on the trajectories of individual droplets.

Also Nijdam et al. [5] compared the Eulerian and Lagrangian approach to include turbulent dispersion and coalescence in a spray. The Reynolds-averaged Navier−Stokes equations together with the $k/\varepsilon$ turbulence model were used to simulate the airflow patterns. The turbulent effect was included within a droplet-parcel transport model using the eddy-lifetime method of Gosman and Loannides [6]. They indicated that the Eulerian approach is more limited than the Lagrangian approach with respect to the range of applicability to multiple systems and ease of implementation. This study included a detailed analysis of the dispersion of droplets in a turbulent system and a comparison of Eulerian and Lagrangian performance. However an investigation on the droplet dynamics and collision outcomes in the presence of turbulent dispersion is missing.

The eddy-lifetime method has the disadvantage that the resulting fluctuating velocity time correlation coefficient is constant over the eddy lifetime, rather than exponentially decaying, and the fluctuating velocity evolution is discontinuous. For the first drawback Ormancey [7] considered the time interval between

subsequent velocity changes as an exponentially-distributed random variable, i.e. a Poisson process. To deal with the unphysical discontinuous fluctuating velocity records, the Langevin stochastic differential equation has been proposed to model the behaviour of fluctuating fluid velocities:

$$d\mathbf{u}^* = -\frac{\mathbf{u}^*}{T_L}dt + \sigma_f\sqrt{\frac{2}{T_L}}d\mathbf{W} \tag{1}$$

where $T_L = C_L k/\varepsilon$ is the Lagrangian (velocity fluctuation) time scale with $C_L$ an experimental constant and $dt$ is an infinitesimal time increment. In isotropic turbulence the droplet Stokes number can be defined as the ratio of droplet response time and time scale of the turbulence $St = \tau_p/T_L$. $\sigma_f$ is the fluid velocity variance and $d\mathbf{W}$ is the Wiener process (white noise). It is a stochastic process of zero mean, a variance (in each Cartesian direction $i$) equal to the time increment,$\langle(dW_i)^2\rangle = dt$, and delta-correlated in the time domain. Formally integrating Eq. 1 over a finite time step $\Delta t$ from the time step $n$ to time step $n+1$, we find:

$$\mathbf{u}^{*n+1} = a\mathbf{u}^{*n} + b\mathbf{e}^n \tag{2}$$

where $\mathbf{e}$ is a random vector, with each Cartesian component $i$ taken from the standard Gaussian distribution, $\langle e_i\rangle = 0$ and $\langle e_i^2\rangle = 1$ and the coefficients $a$ and $b$ are given by:

$$a = \exp\left(-\frac{\Delta t}{T_L}\right) \tag{3}$$

$$b^2 = \sigma_f^2(1-a^2) \tag{4}$$

A detailed explanation of the Langevin approach can be found in Perkins et al. [8], adopted and extended also in the work of Pozorski and Minier [9].

In the work of Breuer and Hoppe [10] the Langevin subgrid scale model was tested for turbulent bubble laden and particle laden flows. It was found that the dispersion only marginally changes the velocity statistics or the volume fraction of the bubbles, possibly due to the small magnitude of the subgrid scale velocities obtained by the Langevin model. Indeed, for a system of smaller solid particles with a Stokes number St=$\tau u_\tau^2/\nu_f$=1.67, based on the response time $\tau$, the wall shear velocity $u_\tau^2$ and the kinematic viscosity $\nu_f$, the influence of the Langevin model on the velocity statistics of the particles is found to be more pronounced. The results showed that the influence of the Langevin subgrid-scale model on the particle velocity fluctuations and the volume fraction increases with decreasing Stokes number. Also Sommerfeld [11] applied the Langevin method to generate the instantaneous fluid velocity fluctuations along the particle trajectory. A considerable over prediction of the frequencies of collisions was observed for particles with St number lower than 10 in case the particle motion was not correlated with the turbulent field.

The prediction of droplet collision outcomes has been the subject of several studies, which started already decades ago. In these studies the characteristics as well as the parameters defining the boundaries between different types of collisions for different fluids and conditions are investigated. When two spherical droplets

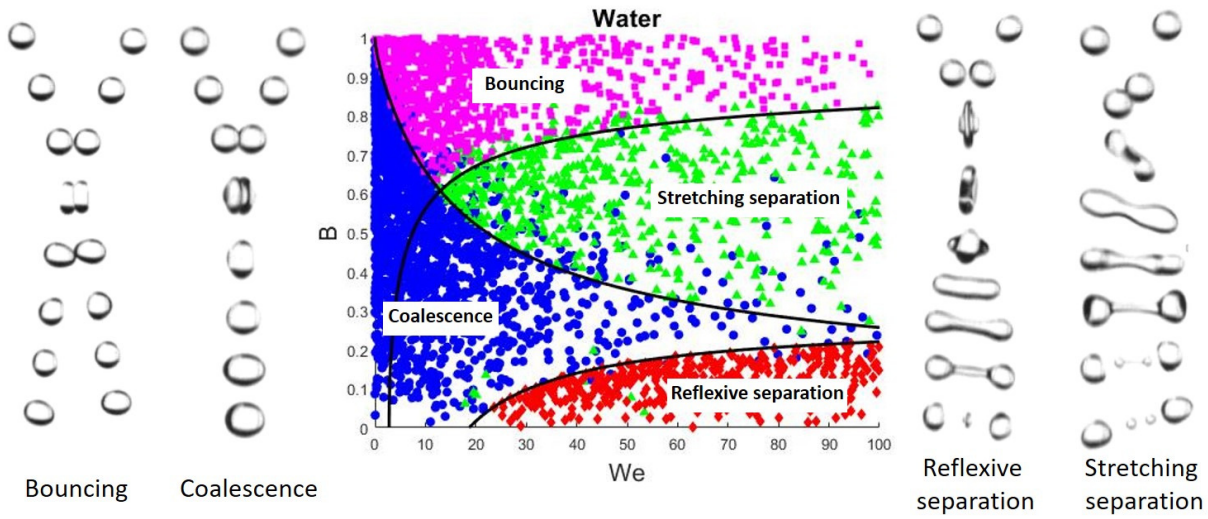


Figure 1: Regime map predicted in the current spray model for water. The numerical collisions for reflexive separation are represented in red diamonds, coalescence in blue circles, stretching separation in green triangles and bouncing in magenta squares. The lines represent the phenomenological model of Ashgriz and Poo [12] and Estrade et al. [13] for $\Delta$=1. Examples of the 4 collision regimes obtained by Finotello et al. [14] experiments are reported.

approach each other, a gas layer is formed in between the surfaces. This layer of compressed gas can be of such high pressure that the drops are unable to make contact, resulting in deformation of both droplets and subsequent bouncing. If two droplets do not bounce and their surfaces make contact, they can permanently form one large droplet by coalescence, or temporarily by reflexive separation or stretching separation. Examples of the experimentally obtained collision regimes and the regime map obtained by simulations are illustrated for water in Fig 1. More details on droplet-droplet collision characterization will be discussed later.

Our current collision outcome boundary models are based on Ashgriz and Poo [12] theory, and have been extended to include viscous dissipation of energy, Finotello et al. [14]. The model of Jiang et al. [15] was one of the first approaches which explicitly included the droplet viscosity as a parameter. They showed that the onset of reflexive separation shifts to higher Weber number (We) as the droplet viscosity to surface tension ratio increases. The model was later refined with the introduction of the Ohnesorge (Oh) number by Qian and Law [16]. Willis and Orme [17, 18] conducted an experimental investigation of viscous droplet collisions in a vacuum environment to avoid aerodynamic effects during collisions. Their results showed a proportional dependency of energy dissipation on droplet viscosity, in contradiction to Jiang et al. [15]. Brenn and Kolobaric [19] extended the model for the prediction of satellite formation after stretching separation of Brenn et al. [20] by including the effect of viscosity. The model gave good predictions for highly viscous liquids and high We numbers, but was not able to describe low viscous liquids

such as water and alcohol. Gotaas et al. [21] studied experimentally and numerically the influence of droplet viscosity and observed that the coalescence to separation boundaries shift to higher We number for fluids with higher viscosity. In the study of Kurt et al. [22] the collision behaviour for pure liquids and suspensions was explored. The number of satellite droplets was found to increase with viscosity for glycerine solutions. The opposite behaviour was noticed for suspensions with solid particles. The authors claimed that a higher concentration of particles may develop perturbations of the combined drop and the break-up of the ligament becomes faster. Also Kuschel and Sommerfeld [23] investigated experimentally the effect of viscosity. The model of Ashgriz and Poo [12] for the coalescence-stretching separation boundary was considered valid by Kuschel and Sommerfeld [23] only for low viscous liquids. For the highly viscous liquids they applied a combination of Ashgriz and Poo [12] and Jiang et al. [15] models. The boundary of coalescence-reflexive separation was observed only at small solid mass fractions. Sommerfeld and Kuschel [24] experimentally extended the previous work of Kuschel and Sommerfeld [23], considering different alcohols and an oil. The derived models are, also in this case, a combination of the Ashgriz and Poo [12] and Jiang et al. [15] models.

Different models for droplet interactions have also been developed based on numerical simulation studies, see e.g Pan and Suga [25], Munnannur and Reitz [26], Nikolopoulos et al. [27]. The growing interest in numerical investigations is due to the advantage of capturing all details of the internal motion of droplets during collision, which is extremely difficult to measure in small scale experiments.

Powders are often manufactured from highly viscous liquid suspensions which are non-Newtonian in nature. Non-Newtonian droplet collisions occur for example during the production of powdered milk. While the studies on Newtonian fluids are numerous, only few are dedicated to non-Newtonian droplet collisions and mostly are based on computational investigations, see Focke and Bothe [28, 29] and Sun et al. [30]. Only in the work of Finotello et al. [31] a complete regime map of shear thinning xanthan is shown. In general these studies show that the collision dynamics is very complex and strongly dependent on the fluid rheology. Given the complexity of non-Newtonian droplet collisions, for the milk collisions investigated in this work we will use experimentally obtained results for the boundaries between different collision outcomes, Finotello et al. [14].

In all the above-mentioned studies, the influence of the sub-grid scale turbulent model on the droplet collision outcomes and on the distribution and frequencies of droplet collision events such as coalescence, separation and bouncing is still not present.

In spray drying the quality of the final product is significantly affected by coalescence and break-up processes. The powder morphology needs to be optimized towards the desired characteristics of the intended product through the control of the atomization, liquid to air flow, collision and drying process. The study of the spray considering all these phenomena is representative of the total system but can result in a very complex investigation. The main aim of our work is to estimate the combined effect of droplet collisions and their response to turbulent dispersion in a spray. Especially coalescence, leading to droplets with larger

sizes, have the bigger influence in the spray performances.

The manuscript is organized as follow. In section 2 the numerical model is described for the dispersed and continuum phase, including a summary of the DSMC method for the detection of droplet collisions and the model to determine the collision outcomes. The operating conditions and geometry of the simulation cases are in section 3. The results are shown and discussed in section 4 together with the verification of the turbulent dispersion model and the boundaries for the collision outcomes. The conclusions are given in section 5.

## 2. Model description

In this study we will use an Euler-Lagrange spray model, based on Direct Simulation Monte Carlo (DSMC) to efficiently handle the droplet collisions. For an extensive description of the DSMC model, see Pawar et al. [32, 33]. The gas phase is treated as continuum and solved on an Eulerian grid and its transport phenomena are computed by solving the volume-averaged Navier-Stokes equations, accounting for the local porosity and the drag force exerted by the droplets. A Lagrangian particle-based model is used for the dispersed phase motion. The detection of droplet collisions is performed applying the stochastic DSMC scheme. In an Eulerian-Lagrangian approach phenomenological models are required to account for various physical processes taking place at subgrid scale. A droplet turbulent dispersion model is needed to estimate the instantaneous fluid velocity fluctuation along the droplet trajectory, which are not calculated explicitly in the conservation equations for the averaged fluid flow.

### *2.1. Gas phase*

The motion of the gas phase is described by the averaged Navier-Stokes equations with two-way coupling for the momentum exchange between the dispersed and continuous phase.

$$\frac{\partial}{\partial t}(\varepsilon\rho_g) + \nabla\cdot(\varepsilon\rho_g\bar{\mathbf{u}}_g) = 0 \tag{5}$$

$$\frac{\partial}{\partial t}(\varepsilon\rho_g\bar{\mathbf{u}}_g) + \nabla\cdot(\varepsilon\rho_g\bar{\mathbf{u}}_g\bar{\mathbf{u}}_g) = -\varepsilon\nabla p - \nabla\cdot(\varepsilon\bar{\tau}_g) + \varepsilon\rho_g\mathbf{g} - \mathbf{S}_p \tag{6}$$

where $\bar{\mathbf{u}}_g$ is the gas velocity, $\rho_g$ the gas density, $\varepsilon$ the gas volume fraction (i.e. porosity), $p$ the pressure and $\bar{\tau}_g$ is the stress tensor. The gas/discrete-phase coupling is accounted for via the drag force term, which is added to the gas momentum equation as a source, $\mathbf{S}_p$:

$$\mathbf{S}_p = \frac{1}{V}\int\sum_{i=1}^{N_d}\frac{\beta V_i}{1-\varepsilon}(\mathbf{u}_g - \mathbf{v}_i)\delta(\mathbf{r}-\mathbf{r}_i)dV \tag{7}$$

where $\mathbf{u}_g = \bar{\mathbf{u}}_g + \mathbf{u}_i^*$ is the local gas velocity near droplet $i$, V is the volume of the cell and $V_i$ the volume of droplet $i$. The delta-function $\delta$ distributes the reaction force on the gas phase to the cells with a trilinear

interpolation. To calculate the inter-phase momentum transfer coefficient , we employed the drag model of Beetstra et al. [34], which is valid for monodisperse and polydisperse systems.

In this study the Vreman [35] subgrid model is used for gas flow effects on the droplet trajectories in Large Eddy Simulations. In LES of turbulent flow, the averaging operator is a linear filtering operator, e.g. a local weighted average over a small volume of fluid. In the averaged Navier-Stokes equations additional terms appear, for which a model has to be assumed before the equations can be solved. The additional terms in the momentum equations are spatial derivatives of the turbulent stress tensor. In a large-eddy simulation this tensor is modelled with a subgrid model, so called since the scales which can be represented on the grid are solved explicitly, while the effect of the small subgrid scales is modelled.

The effect of LES turbulence on the filtered gas velocity is taken into account through a stress model, Vreman [35] which increases the effective gas viscosity:

$$\overline{\tau}_g = -\nu \left( (\nabla \bar{\mathbf{u}}_g) + (\nabla \bar{\mathbf{u}}_g)^T - \frac{2}{3}(\nabla \cdot \bar{\mathbf{u}}_g)\mathbf{I} \right) \tag{8}$$

$$\nu = \nu_{laminar} + \nu_e \tag{9}$$

The eddy viscosity for turbulent shear flow is formulated with the following correlation (Einstein summation implied over Cartesian indices $i$ and $j$):

$$\nu_e = \rho_g c \sqrt{\frac{B_\beta}{\alpha_{ij}\alpha_{ij}}} \tag{10}$$

$$\alpha_{ij} = \frac{\partial \bar{u}_j}{\partial x_i} \tag{11}$$

$$B_\beta = \beta_{11}\beta_{22} - \beta_{12}^2 + \beta_{11}\beta_{33} - \beta_{13}^2 + \beta_{22}\beta_{33} - \beta_{23}^2 \tag{12}$$

$$\beta_{ij} = \Delta_m^2 \alpha_{mi}\alpha_{mj} \tag{13}$$

where $\Delta_m$ is the cell grid size in the $m$ direction. The theoretical subgrid dissipation is proportional to the subgrid kinetic energy $k$, taking $c_1 = 2\sqrt{2}$:

$$k = c_1 \nu_e ||S|| = 2\nu_e |S| = 2\nu_e \sqrt{2 S_{ij} S_{ij}} \tag{14}$$

$$S_{ij} = \frac{1}{2}\left( \frac{\partial \bar{u}_i}{\partial x_j} + \frac{\partial \bar{u}_j}{\partial x_i} \right) \tag{15}$$

For LES the subgrid turbulent motion is usually assumed to be locally homogeneous and isotropic, leading to a relation between subgrid velocity and kinetic energy:

$$u_{sgs} = \sqrt{\frac{2}{3}k} \tag{16}$$

*2.2. Droplet dynamics and turbulent dispersion*

In the Lagrangian approach the equations of motion of each droplet are given by:

$$\frac{d\mathbf{r}_p}{dt} = \mathbf{v}_p \tag{17}$$

$$\frac{d\mathbf{v}_p}{dt} = \frac{\mathbf{u}_{rel}}{\tau_p} - \frac{\nabla p}{\rho_p} + \mathbf{g} \tag{18}$$

where the droplet dynamic relaxation time is:

$$\tau_p = \frac{d^2 \rho_l}{18 \mu_g f(Re)} \tag{19}$$

and $\mathbf{u}_{rel} = \mathbf{u}_g - \mathbf{v}_p$ with $\mathbf{u}_g = \bar{\mathbf{u}}_g + \mathbf{u}_p^*$. $\mathbf{u}_g$ is the gas velocity at the droplet location, $\bar{\mathbf{u}}_g$ is the filtered resolved velocity and $\mathbf{u}_p^*$ the stochastic subgrid velocity at the location of particle $i$. $f(Re)$ is the drag factor. The subgrid velocity Langevin stochastic differential equation is updated according to:

$$\mathbf{u}^{*n+1} = \left(1 - \frac{\Delta t}{\tau_L^*}\right) \mathbf{u}^{*n} + u_{sgs} \sqrt{\frac{2\Delta t}{\tau_L^*}} \zeta \tag{20}$$

with $u_{sgs}$ given by Eq. 16 and $\tau_L^*$ the Lagrangian time scale is given by :

$$\tau_L^* = \frac{\tau_{sgs}}{\sqrt{1 + \vartheta^2}} \tag{21}$$

Here $\tau_{sgs} = C_{sgs}\Delta / u_{sgs}$ is the characteristic subgrid time scale and $\vartheta = |\bar{\mathbf{u}} - \mathbf{v}_p| / u_{sgs}$ is the normalized drift velocity. $C_{sgs}$ is an empirical constant equal to 0.1, [36]. The random vector $\zeta$ is obtained from a isotropic 3D Gaussian distribution with mean 0 and standard deviation (in each Cartesian direction) of 1. In case $\Delta t > \tau_L^*$ the new residual velocity is directly obtained from $\mathbf{u}^* = u_{sgs}\zeta$. For simplification we do not distinguish between characteristic time scales for the parallel and perpendicular direction, see Irannejad and Jaberi [37], which occurs only for large particles.

*2.3. Droplet detection and collision outcomes*

Direct Simulation Monte Carlo (DSMC) was introduced by Bird [38] and later applied to two impinging droplet sprays by Du et al. [39]. Below we present the main features of our modified DSMC method. For details the reader is referred to Pawar et al. [32]. With this approach, a group of droplets, a parcel, is represented by a single droplet. Only the trajectories of these representative droplets need to be calculated and collisions are detected stochastically rather deterministically, which reduces computation time.

The first part of the algorithm is the search for a collision partner. In this version of DSMC, we use a local spherical searching scope, $R_{s,i}$, within which a droplet of diameter $d_i$ searches for its colliding partners. The droplet time step is updated by calculating the mean free path of each moving droplet $L_i = |\mathbf{v}_i| / f_i$, where the collision frequency is:

$$f_i = \sum_{j \in R_{s,i}} |v_{ij}| \frac{\pi}{4} (d_i + d_j)^2 \frac{n_j}{\frac{4}{3}\pi R_{s,i}^3} \tag{22}$$

where $j$ stands for the droplet within the searching scope of the droplet $i$, $|v_{ij}|$ is the magnitude of the relative velocity, $\frac{\pi}{4}(d_i + d_j)^2$ is the effective collision area, $\frac{4}{3}\pi R_{s,i}^3$ the volume of the searching scope and $n_j$ the real number of droplets represented by the parcel $j$, or parcel size. During one droplet time step $\Delta t_{d,i}$, the probability of droplet collision should be less than 1. This condition, known as the principle of uncoupling, is necessary to separate calculations of inter-droplet collisions from those of free droplet motion. Because the droplet time step can be at maximum equal to the gas phase time step, we choose $\Delta t_{d,i} = min\left[\frac{L_i}{3v_i}, \Delta t_g\right]$.

Having determined the droplet time step, the DSMC algorithm proceeds with the choice of the collision partner. The collision probability between a specific pair of droplets $i$ and $j$ is:

$$P_{ij} = |v_{ij}|\frac{\pi}{4}(d_i + d_j)^2 \frac{n_j \Delta t_{d,i}}{\frac{4}{3}\pi R_{s,i}^3} \tag{23}$$

According to the Nambu method, [40], an actual collision is performed only if $\chi > \frac{j}{N_i} - P_{ij}$ where $\chi$ is a random number with uniform distribution between 0 and 1, $j$ is the candidate collision partner chosen as $j = int[\chi N_i] + 1$ and $N_i$ is the total number of droplets in the searching scope of $i$.

We assume the simultaneous collisions between three or more droplets can be neglected because of the low liquid to air volume fraction of the spray. In the work of Hinterbichler et al. [41], ternary droplet collisions were investigated experimentally. The morphology of collision events between three droplets and their boundaries between the collision outcomes resulted similar to the ones of binary droplet collisions. Once the collision pair is determined, the outcome of the binary collision needs to be predicted. Phenomenological models for the collision outcome are provided as a function of Weber number, Ohnesorge number and impact parameter. The first two numbers can be calculated based on liquid density, droplet diameter, surface tension, viscosity and the relative velocity. The Weber number is the ratio between inertial forces and surface tension:

$$We = \frac{\rho_d d_s |v_{ij}|^2}{\sigma} \tag{24}$$

where $\rho_d$ is the droplet density, $d_s$ is the diameter of the smallest droplet, and $\sigma$ is the surface tension. The ratio between $d_s$ and the large droplet diameter $d_l$ is the size ratio $\Delta$.

The impact parameter B is defined, before the moment of impact, as the distance b between the two droplet centres in the plane perpendicular to the relative velocity vector, normalized by the average droplet diameter.

$$B = \frac{2b}{d_s + d_l} \tag{25}$$

When B is equal to 0 it is a head-on collision and when it is 1 a grazing collision.

The impact parameter, however, cannot be determined deterministically for each specific collision, since the DSMC simulation does not specifically track the trajectories of all individual droplets. Therefore, it is assumed that droplets collide at random positions, in which case the normalized probability distribution for

a certain impact parameter is given by $P(B) = 2B$. This can be generated by choosing $B = \sqrt{\xi}$ with $\xi$ a uniform random number between 0 and 1. Note that lower impact parameters have a lower probability. The position of the Weber number with respect to the critical Weber numbers for reflexive separation and stretching separation, determines the collision outcome.

In case of coalescence, the smallest droplet is removed from the simulation and the size of the larger droplet is increased, based on conservation of mass. In case of reflexive separation and stretching separation, one or more new (satellite) droplets are generated. Consequently, the mass and volume of the parent droplets is reduced. A model predicting the number and size of the satellite droplets was adapted from Ko et al. [42]. In all cases, a momentum balance is used to calculate the new velocities after collision.

To account for the droplet viscosity the Ohnesorge number (Oh) is used, which represents the ratio of viscous forces and the combined effect of inertial forces and surface tension:

$$Oh = \frac{\mu_d}{\sqrt{\rho_d d_s \sigma}} \tag{26}$$

where $\mu_d$ is the droplet fluid viscosity.

For water sprays the boundary collision model of Ashgriz and Poo [12] is applied for the boundaries demarcating coalescence and stretching separation as well as reflexive separation. For the bouncing regime the Estrade et al. [13] is used. In Fig 1 the regime map used in the simulations is illustrated for water together with the 4 collision regimes. Some collisions are outside their regime because in the simulation they are not occurring always at $\Delta$=1. For representing the models we chose a fixed size ratio of 1. For milk concentrates we use Finotello et al. [14] model expressed as:

$$We_{reflexive} = 3\left[7\left(1+\Delta^3\right)^{2/3} - 4\left(1+\Delta^2\right)\right] \frac{\Delta\left(1+\Delta^3\right)^2}{\left(\Delta^6\eta_1+\eta_2\right)} + W_{translation} \tag{27}$$

$$We_{translation} = We_{milk,crit} - We_{water,crit} \tag{28}$$

$$We_{milk,crit} = 17.05 + 510 \cdot Oh \tag{29}$$

Here $\eta_1$ and $\eta_2$ are geometric factors as introduced by Ashgriz and Poo [12].

$$We_{stretching} = \left[\frac{3.0}{B}\left(1 + 0.05\frac{\mu}{\sigma}\sqrt{\frac{\rho d}{\sigma}}\right)\right]^2 \tag{30}$$

## 3. Numerical simulation geometry and parameters

In the numerical spray model new droplets are introduced from a hollow cylindrical shell. Droplets are assumed to be spherical and released with an angle direction linearly proportional to the radial direction so that the axial and radial velocities are: $v_{zi} = v_{inj}\cos\left(2r_i\theta/d_{out}\right)$ and $v_{ri} = v_{inj}\sin\left(2r_i\theta/d_{out}\right)$ where $v_{inj}$ is

| **Parameters** | Symbols | **Values** |
|---|---|---|
| Number of Eulerian cells | NX x NY x NZ | 60x60x120 |
| System width [m] | Lx | 0.6 |
| System depth [m] | Ly | 0.6 |
| System height [m] | Lz | 1.2 |
| Mass flow rate [kg/s] | q | 0.1275 |
| Nozzle radius [m] | $r_{nozzle}$ | 0.889 $\times 10^{-3}$ |
| Rosin-Rammler spreading parameter | n | 3.5 |
| Inlet droplets velocity [m/s] | $v_{inj}$ | 200 |
| Initial Sauter mean droplet radius [m] | $r_{mean}$ | 25.5 $\times 10^{-6}$ |
| Cone nozzle spray angle [degree] | $\theta$ | 81 |
| Parcel size | $n_i$ | 1500 |
| Typical number of droplets in the system | | $10^9$ |

Table 1: Numerical simulation parameters

the initial nozzle injection velocity, $d_{out}$ is the outer cone diameter, $\theta$ is the spray cone angle and $r_i$ is the radial position of the drop from the symmetry axis of the spray. For many real sprays, the Rosin-Rammler distribution predicts the droplet size distribution. The mass fraction of all the droplets with a diameter smaller than d, Y(d), is equal to:

$$1 - Y(d) = \exp\left[-\left(\frac{d}{\overline{d}}\right)^{n_s}\right] \tag{31}$$

where $\overline{d}$ is the Rosin-Rammler diameter and $n_s$ is the spreading parameter, set equal to 3.5 as in the work of Madsen [43]. New droplets are introduced in a cylindrical region until the introduced cumulative mass is equal to the desired total mass for the given time step. Droplet diameters are generated in accordance with Eq.31 by generating a uniform random number $\xi$ between 0 and 1 and then choosing $d = \overline{d}\,(-ln\xi)^{\frac{1}{n_s}}$. The smallest droplets whose collective masses are 0.5% of the total injected mass as well as the biggest droplets with a collective mass of 0.5% of the total mass are excluded. Additionally, the random number $\xi$ has to be smaller than $(d_{0.5\%}/d)^3$ because the *number* of droplets in a Rosin-Rammler distribution, which is a cumulative *mass* probability, scales with $d^{-3}$.

In the Lagrangian method a single particle in the simulation is representative of a large number of real particles in the spray. In this work a simulated droplet is representative of 1500 droplets.

In Tab. 1 simulations parameters are given. The initial spray cone angle, the mass flow rate and the initial average droplet size are based on the experimental data in the work of Pawar et al. [33]. In the spray dryer model, the nozzle is placed 20 cm from the top wall of the rectangular domain. For the domain

| **Liquids** | Droplets density [kg/m$^3$] | Droplets viscosity [Pas] | Droplets surface tension [N/m] |
|---|---|---|---|
| Water | 1000 | 0.001 | $73{\cdot}10^{-3}$ |
| Milk 20% TS | 1041 | 0.0043 | $46.8{\cdot}10^{-3}$ |
| Milk 46% TS | 1094 | 0.083 | $46.9{\cdot}10^{-3}$ |
| Reference fluid | 1094 | 1.2 | $48{\cdot}10^{-3}$ |

Table 2: Physical properties of the liquids.

boundary conditions a prescribed pressure of 1 bar is used. The boundaries allow for inflow and outflow of gas. Droplets are immediately eliminated when the system boundaries are crossed. The gas flow is self-induced by the droplet motion.

We checked the effect of grid size and parcel number on the droplet size distribution. The results are invariant for a refined grid size of 80x80x140 and for a parcel number of 2500.

In Tab. 2 the physical properties of the liquids used in this work are reported. In Fig. 2 schematics of the system used for the verification case of the turbulence dispersion model and for the simulation of the spray system are shown.

## 4. Results and discussion

Initially we verify the implementation of the Langevin equation for the residual velocity analysing the kinetic energy of the droplets. With the inclusion of the turbulent dispersion model, the changes on the droplet phase in terms of number and frequencies of collisions are discussed. The implementation of the collision outcome boundaries for viscous liquids are then verified by representing the respective regime maps. The droplet-droplet collision outcomes in the spray are analysed in terms of non-dimensional parameters. We expect that the combined processes of collisions and dispersion have a relevant effect on the spray dynamics.

The droplet probability distribution function (PDF) or probability density function indicates the total mass or total volume of all the droplets belonging to a certain size class. $m(d)\Delta d$ is the fractional mass of the droplets whose diameters are in the range $[d, d+\Delta d]$. The mass- or volume- averaged PDF is preferable to a PDF based on number of particles in a certain size, because it avoids the emphasis of smaller droplets over the entire population, which however contribute relatively little to the total droplet mass.

To demonstrate that the droplet size distributions are statistically correct and not influenced by the finite simulation time during which the distributions are calculated, a time dependency analysis, depicted in Fig. 3 for two different positions in the spray, is performed. The distribution in Fig. 3a is narrow while the one in Fig. 3b is broader. Far from the inlet region the droplets significantly grow in size due to the

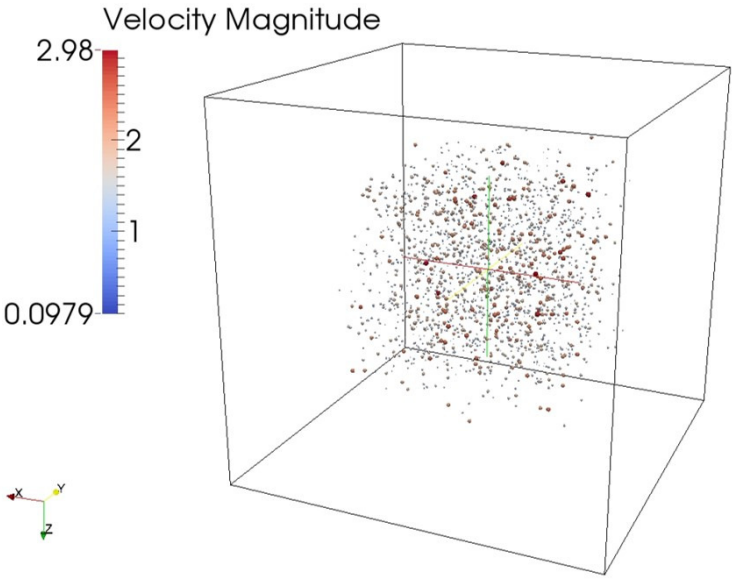


(a)

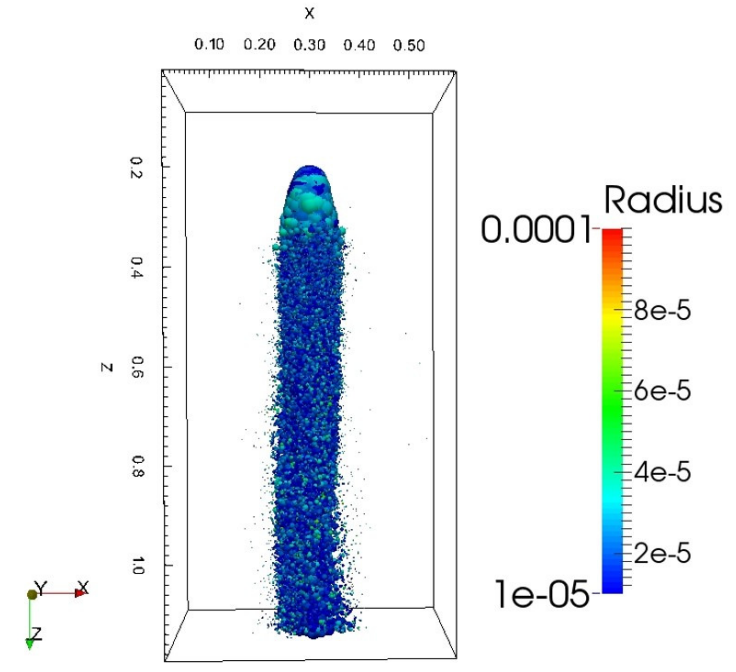


(b)

Figure 2: Schematic of the system used for the verification case of the turbulence dispersion model (a) and for the simulation of the spray system (b).

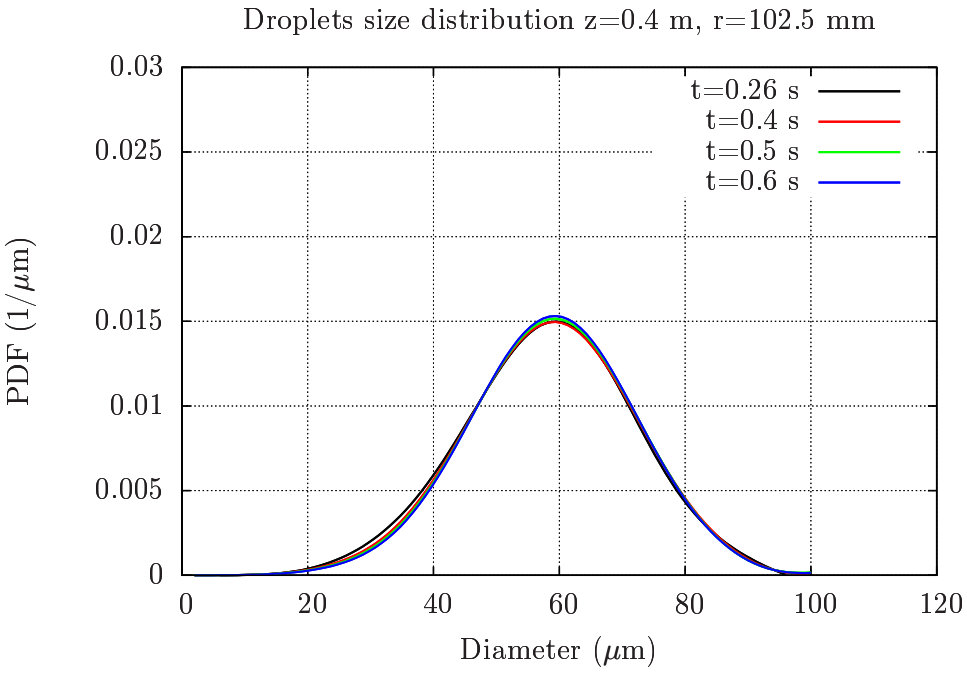


(a)

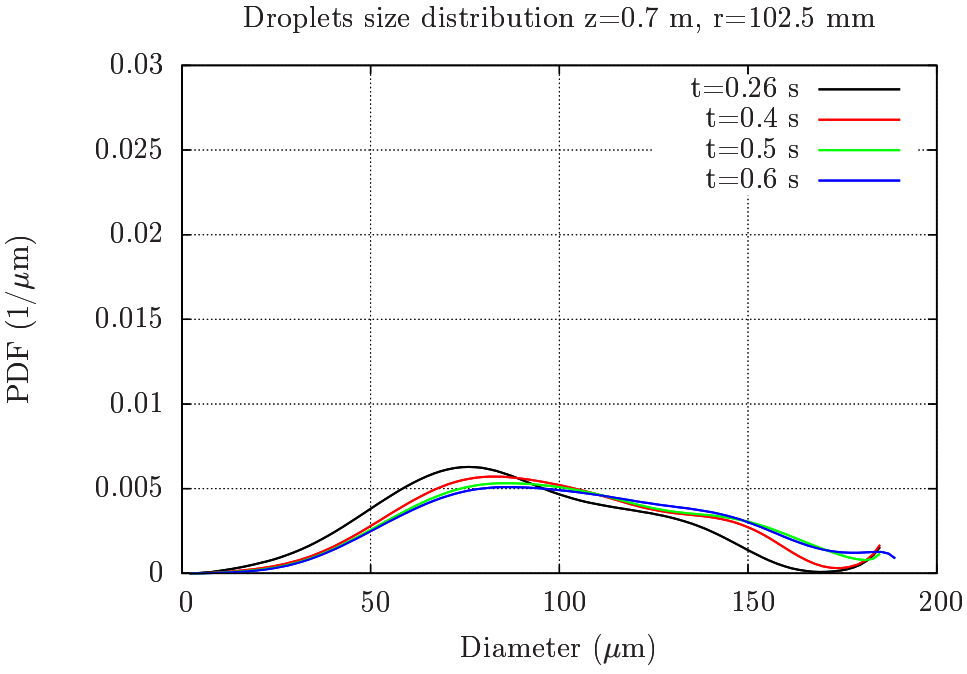


(b)

Figure 3: Time dependency analysis on the droplet distribution function.

predominance of coalescence over separation events caused by the reduction in relative velocity. In this region the spray is less dense and the droplet sizes ranges from very small, 10 $\mu$m, to very large, 200 $\mu$m. For both cases the measurement time has no influence after 0.26 s. This demonstrates that the number of drops in these locations is measured for a sufficient long time to obtain results statistically representable of the distributions. All the simulations of this work have a total simulation time of 0.3 s.

### *4.1. Verification of the turbulent dispersion model*

The verification of the turbulent dispersion model is performed by measuring the turbulent kinetic energy of the droplets in a known random turbulence field and comparing with analytical results. A number of 2000 drops are placed randomly in a spherical configuration in a cubic domain, see Fig. 2a. The drops disperse in a homogeneous and isotropic turbulent flow. For this test the filtered velocity of the gas $\bar{\mathbf{u}}$ is set hard to zero, and the subgridscale velocity $u_{sgs}$, instead of being updated with the turbulent kinetic energy, is set to 2 m/s or 4 m/s, respectively. The particles also have a zero initial particle velocity $\mathbf{v}_p(t=0)=0$. Here we focus on a single Cartesian component of the fluctuation velocity. Given that this fluctuating velocity at time $n$ is $u^{*n}$ it easy to show that the expected mean square fluctuating velocity at time $n+1$ is :

$$\langle \mathbf{u}^{*n+1} \cdot \mathbf{u}^{*n+1} \rangle = \left(1 - \frac{\Delta t}{\tau_L^*}\right)^2 \langle \mathbf{u}^{*n} \cdot \mathbf{u}^{*n} \rangle + \frac{2\Delta t}{\tau_L^*} u_{sgs}^2 \tag{32}$$

So the kinetic energy $k = \left\langle (\mathbf{u}^*)^2 \right\rangle$ associated with the fluctuating velocity, the residual kinetic energy, should evolve according to the above equation.

The particle or droplet will respond to the time-dependent fluctuating gas velocity according to:

$$\frac{d\mathbf{v}_p}{dt} = \frac{1}{\tau_s}(\mathbf{u}^* - \mathbf{v}_p) \tag{33}$$

$$\tau_s = \frac{m}{\beta V_p} \tag{34}$$

Formally integrating the Langevin equation for the fluctuating gas velocity $\mathbf{u}^*$, and solving the equation of motion of the particle, it is possible to find an analytical solution for the expected evolution of the kinetic energy of the particle. For an initial particle velocity $\mathbf{v}_p = 0$ and initial fluctuating gas velocity $\mathbf{u}^* = 0$ the solution is:

$$\langle \mathbf{v}_p \cdot \mathbf{v}_p \rangle = 3u_{sgs}^2 \frac{1}{(1+\mathrm{St})(1-\mathrm{St})^2} \left[ (1-\mathrm{St})^2 - \mathrm{St}\,(1+\mathrm{St})\,\mathrm{e}^{-2t/\tau_s} + 4\mathrm{St}\mathrm{e}^{-(1+\mathrm{St})t/\tau_s} - (1+\mathrm{St})\,\mathrm{e}^{-2\mathrm{St}t/\tau_s} \right] \tag{35}$$

where $\mathrm{St} = \tau_s/\tau_L$ is the Stokes number. A detailed explanation of Langevin equation and solutions of equations of this kind can be found in Coffey and Kalmykov [44]. The above analytical solution for the kinetic energy of the particles $k_p$ has been found by assuming the friction $\beta$ and therefore the droplet response

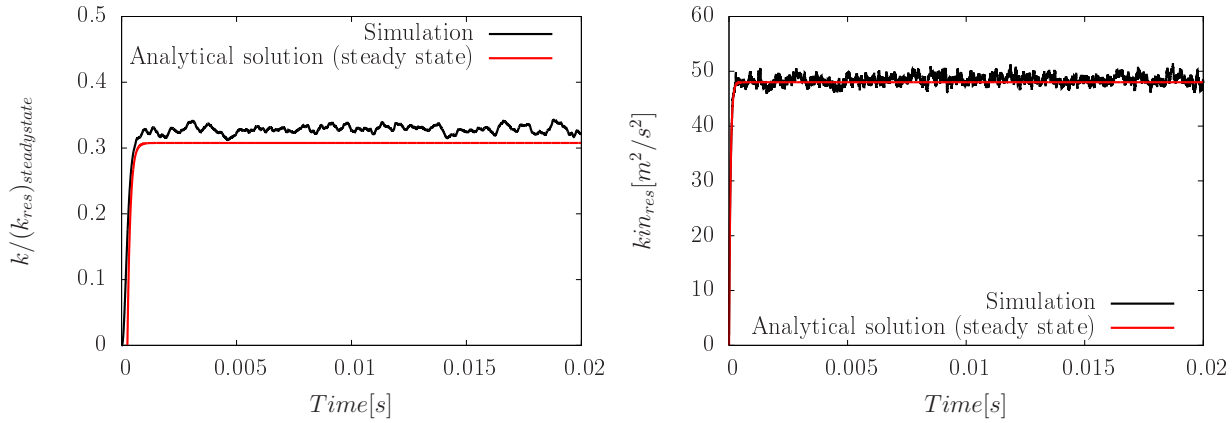


Figure 4: Particle kinetic energy and residual kinetic energy of the simulation for $u_{sgs}$=4 m/s, St=2.23, $Re_p$=4.

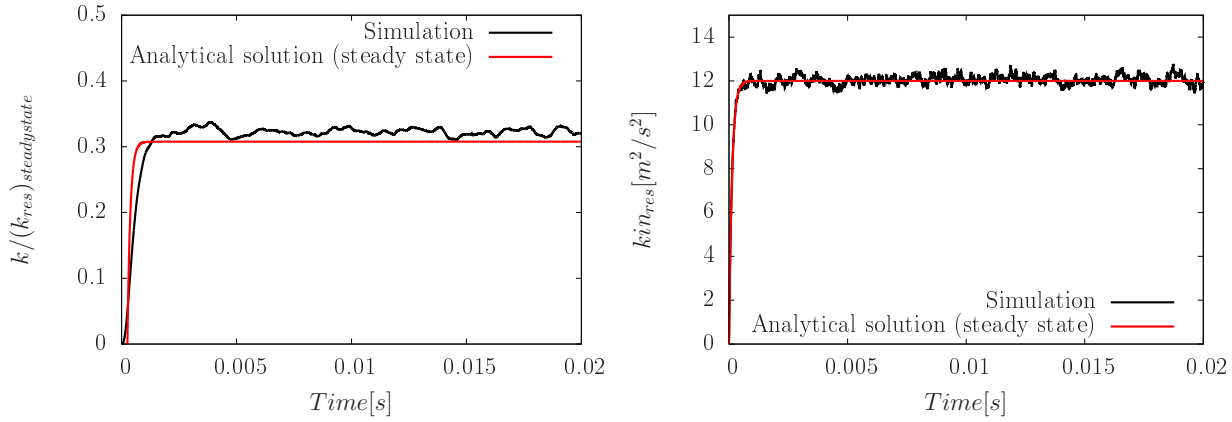


Figure 5: Particle kinetic energy and residual kinetic energy of the simulation for $u_{sgs}$=2 m/s, St=2.25, $Re_p$=1.

time $\tau_s$ is constant so it is not compatible with the measured $k_p$ in case the friction factor $\beta$ is changing in time. However in the steady state, we can estimate the characteristic relative velocity, and therefore the characteristic values of $\beta$ and $\tau_s$. From the above analytical equation, we expect in the steady state:

$$\lim_{t\to\infty} \langle \mathbf{v}_p \cdot \mathbf{v}_p \rangle = 3u_{sgs}^2 \frac{1}{1+\mathrm{St}} \tag{36}$$

with $St = \tau_s/\tau_L$ the Stokes number expressing the ratio of the particle relaxation time to the Lagrangian (eddy) relaxation time.

In Fig.4 the kinetic energy of the particle is shown for St=2.23 and Reynolds number of 4 for $u_{sgs}$=4 m/s together with the residual kinetic energy. Although not reported here, we performed the same analysis also for other particles sizes keeping constant the subgrid scale velocity. Another example of kinetic energy and residual kinetic energy for a subgrid velocity of 2 m/s, St=2.25 and Re=1 is illustrated in Fig. 5. The residual kinetic energy $k_{res}$ predicted by the simulations corresponds to the analytical solution for all cases.

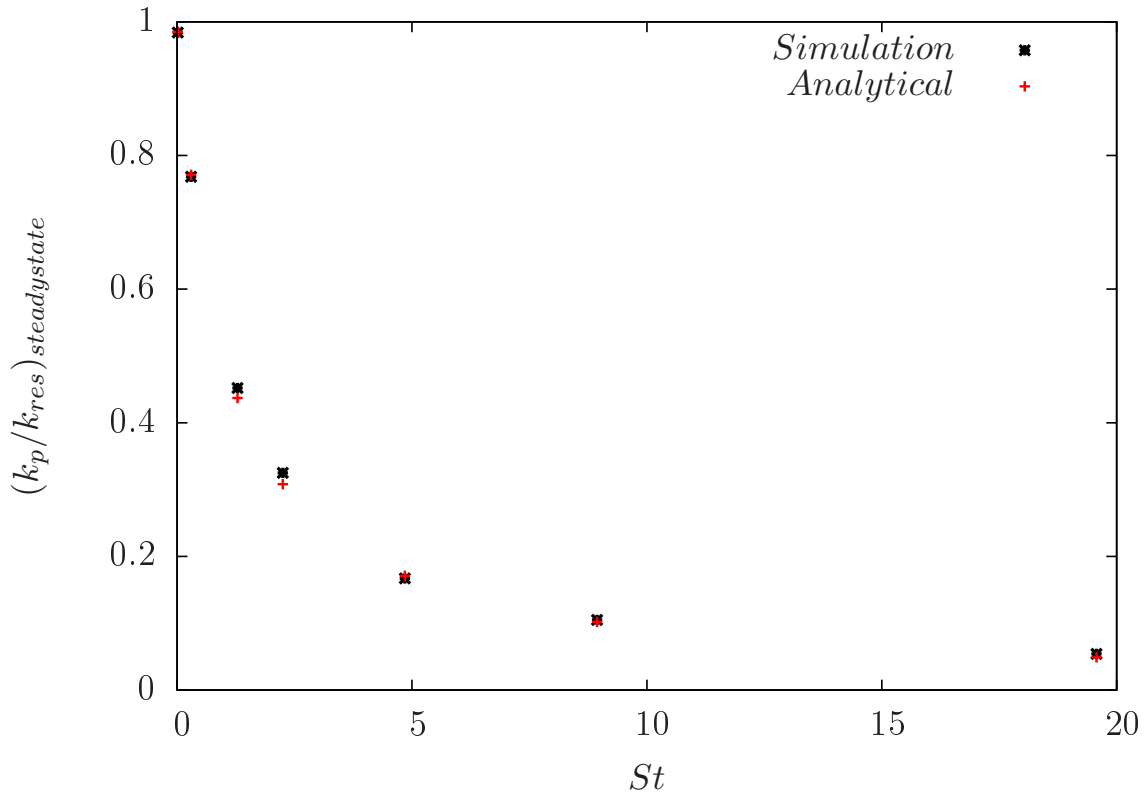


Figure 6: Ratio of particle to residual kinetic energy at steady state as a function of the St number. The expected the analytical ratio is 1/(1+St).

The calculated particle kinetic energy $k_p$ has been normalized by the steady state solution of the residual kinetic energy $(k_{res})_{steadystate} = 3u_{sgs}^2$ to be compared to the steady state analytical solution. This is due to the fact that the analytical solution was derived assuming that the drag factor $\beta$ remains constant in time.

Fig. 6 shows the steady state solution of the normalized particle kinetic energy compared to the steady state analytical solution 1/(1+St) for different St numbers. A good agreement of the calculated particle kinetic energy with the analytical solution characterizes the entire range of Stokes number. For very small droplets the Lagrangian time scale assumption $\tau_L^*=\tau_{sgs}$ has been used while for larger droplet diameters $\tau_L^*=\frac{\tau_{sgs}}{\sqrt{1+\vartheta^2}}$. In the considered case of $u_{sgs}$=2 m/s the critical $St_{crit}$ number demarcating the first and second assumption for $\tau_L^*$ is around 2.

*4.2. Effect of turbulence dispersion on the frequency of collisions*

The effect of the dispersion model on the spray can be evaluated by comparing the size distributions at different location in the spray with or without inclusion of the turbulence dispersion model. It is expected

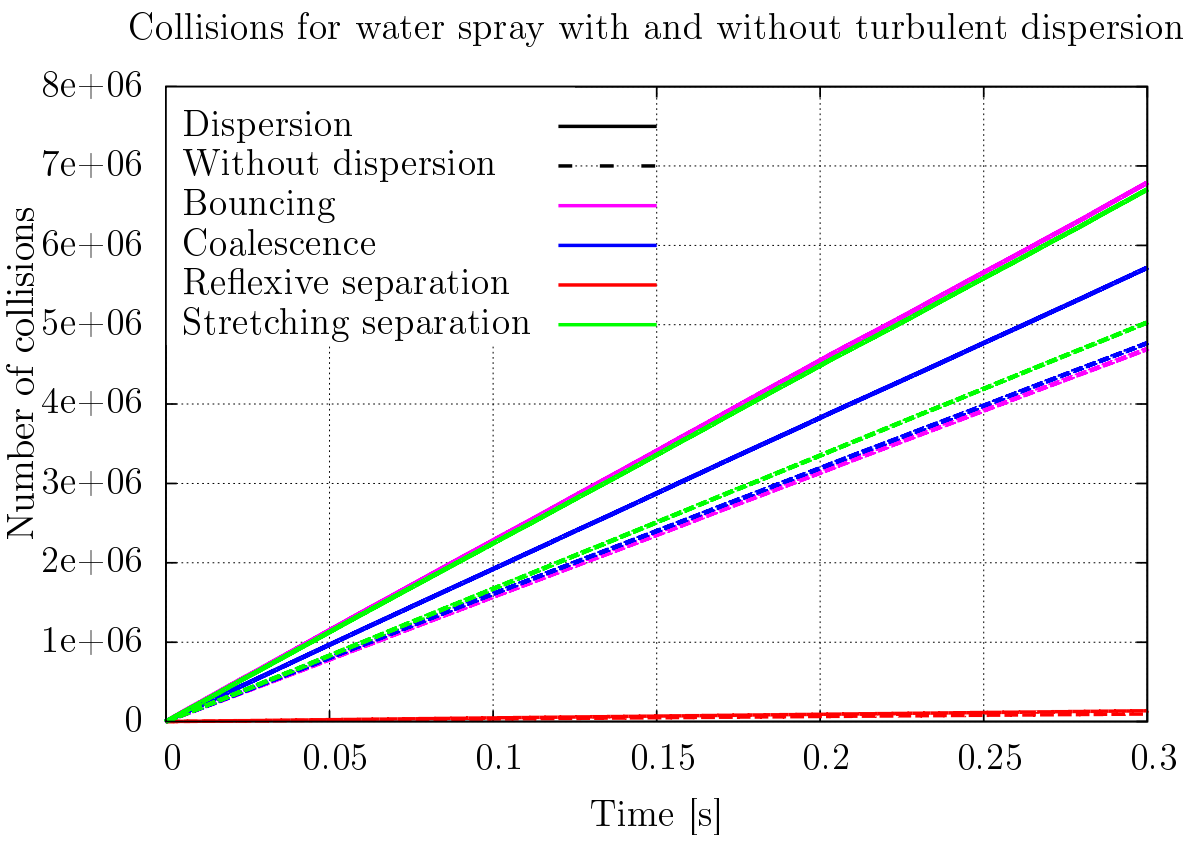


Figure 7: Number of collisional events for water spray with and without turbulent dispersion model, separated by collision type B=bouncing,C=coalescence, SS=stretching separation, RS=reflexive separation.

that differences in the size distribution function will occur mainly at small droplet diameter rather than large diameter, because larger droplets are less correlated with the motion of the gas flow. Small droplets are more responsive to turbulent fluctuations and therefore expected to collide more frequently when the turbulent dispersion model is included. More generally, we expect that the number of collisions in a simulation of a spray with turbulent dispersion will be higher than without dispersion, as confirmed in Fig.7. In particular the regimes of bouncing and stretching separation are enhanced. This is consistent with the increase of the relative velocities and therefore of the range of We numbers so that, as can be predicted from the regime map in Fig.1, these two types of collision events are more likely to happen. Note that the reflexive separation occurs only in case of near head-on impact, which has a lower probability compared to grazing collisions. For this reason the increase of the reflexive breakups is not significant in relation to the others collision outcomes.

In Fig.8 the frequency of collisions leading to bouncing, coalescence, reflexive and stretching separation of water and milk 20% droplets are shown as a function of radial distance from the central symmetry axis to the edge of the spray, at an axial position of 10 cm from the droplet inlet for the cases with and without turbulence dispersion. For all the simulated cases the measurement time was 0.3 s to obtain statistically accurate results. The turbulent dispersion model has a strong influence on the rate of inter-droplet collisions for both water and milk because the velocity fluctuations are higher. In general it can be observed that close to the axis of the spray the frequency of collisions is low because of the lower droplet number density in the central region of the hollow-cone spray. But it is in the vicinity of the axis that the effect of dispersion is more pronounced rather than at larger radial coordinates, because the turbulent intensity is highest inside the hollow cone spray. This explains why the dispersion model does not strongly influence the initial cone angle and spray width.

The comparison with actual spray experiments shows very similar air flow velocity field to the one obtained by Pawar et al. [33]. In their work, the droplet size and velocity distributions were measured using a Phase Doppler Interferometry (PDI) system. This optical technique does not allow the measurements of air velocities. Moreover the technique has some limitations in measuring droplet velocities and diameters in the positions close to the atomizer because of the high liquid volume fraction.

The mass-averaged velocity of the droplets and of the velocity of the air, simulated in this work, are shown in Fig.9 together with the droplet velocities obtained by the experiments reported by Pawar et al. [33]. Initially the droplet velocity is very high (more than 100 m/s), but the air drag causes a fast deceleration. We observe that the velocity is still relatively high near the central axis, but decreases rapidly with increasing distance from the central axis. The velocity magnitudes and directions observed in the simulations are in semi-quantitative agreement with the experimental measurements. The inclusion of the turbulent dispersion model does not influence the overall fluid flow field.

While the mean and fluctuations flow velocity are not affected by the turbulent dispersion model, we

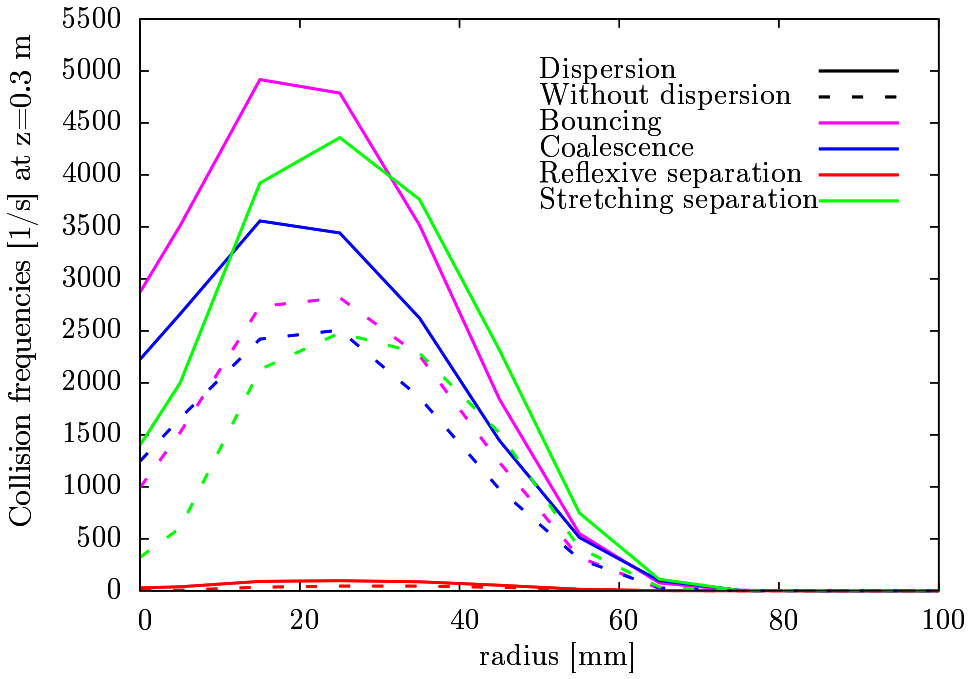


(a) Water

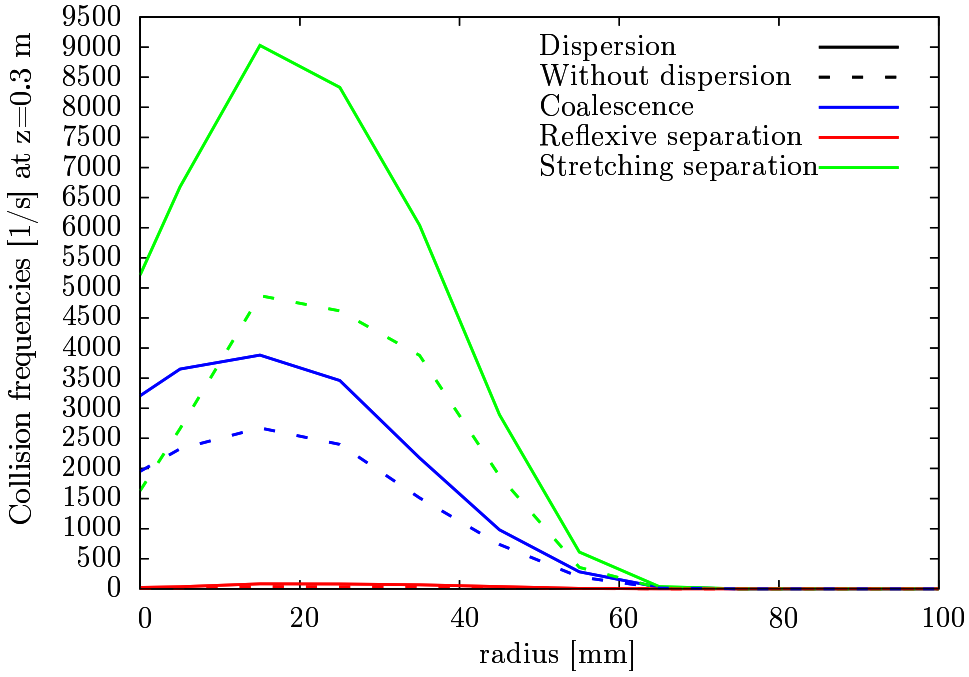


(b) Milk 20%

Figure 8: Frequency of collisions for (a) water and (b) milk 20 % with and without turbulent dispersion model as a function of radial distance from the central symmetry axis, at an axial position of 10 cm from the droplet inlet. B=bouncing,C=coalescence, SS=stretching separation, RS=reflexive separation.

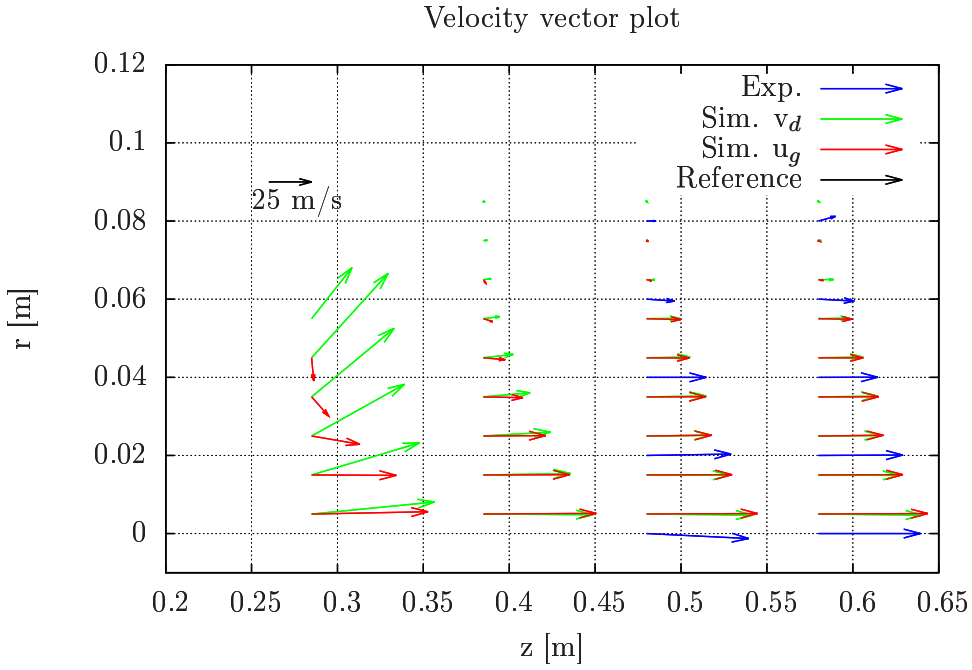


Figure 9: Mass averaged droplet velocity $v_d$ vector obtained by simulation of this work and experiments of Pawar et al. [33], and induced gas velocity $u_g$ vectors in different locations of the spray.

observed an increase of the total number and frequencies of collisions. Indeed the droplet collision depends on the relative velocity and not on the mean or fluctuations of the air velocity flow. Tab. 3 shows the mean relative velocity $v_{rel}$ at the moment of impact of the droplets for different collision outcomes in presence or absence of turbulent dispersion model. The mean is calculated over the total number of collisions in the spray till the simulation time of t=0.3 s. The increase of collisions in presence of turbulent dispersion model is due to a slight enhancement of the relative velocities between the droplets.

### *4.3. Verification of the droplet-droplet collisional model*

To verify a correct implementation of the boundaries between different collision outcomes, we consider three simulations to reproduce the regime maps found for milk 20%, 30% and 46% TS content reported in the study Finotello et al. [14]. In these experiments, binary droplet collisions of the same size ($\Delta = 1$) are carried out through generation of mono dispersed droplets brought to impact. In a spray the atomized droplets at the inlet do not all have the same size. Therefore when colliding we generally have $\Delta \neq 1$, as we will show more in detail later in this paper. Because the droplet size varies, the boundaries between the regimes can be observed to shift.

Fig. 10 illustrates the simulated collision outcomes in a spray as a function of We number and impact parameter B. The markers represent numerical collisions with Ohnesorge numbers in the same range as the

Table 3: Average collisional relative velocities $v_{rel}$ with and without turbulent dispersion model.

| Case | $v_{rel,avg}$ m/s for Coalescence | $v_{rel,avg}$ m/s for Stretching separation | $v_{rel,avg}$ m/s for Reflexive separation | $v_{rel,avg}$ m/s for Bouncing |
|---|---|---|---|---|
| Water with dispersion | 5.99 | 20.62 | 16.6 | 10.32 |
| Water without dispersion | 4.35 | 19.49 | 16.09 | 10.3 |

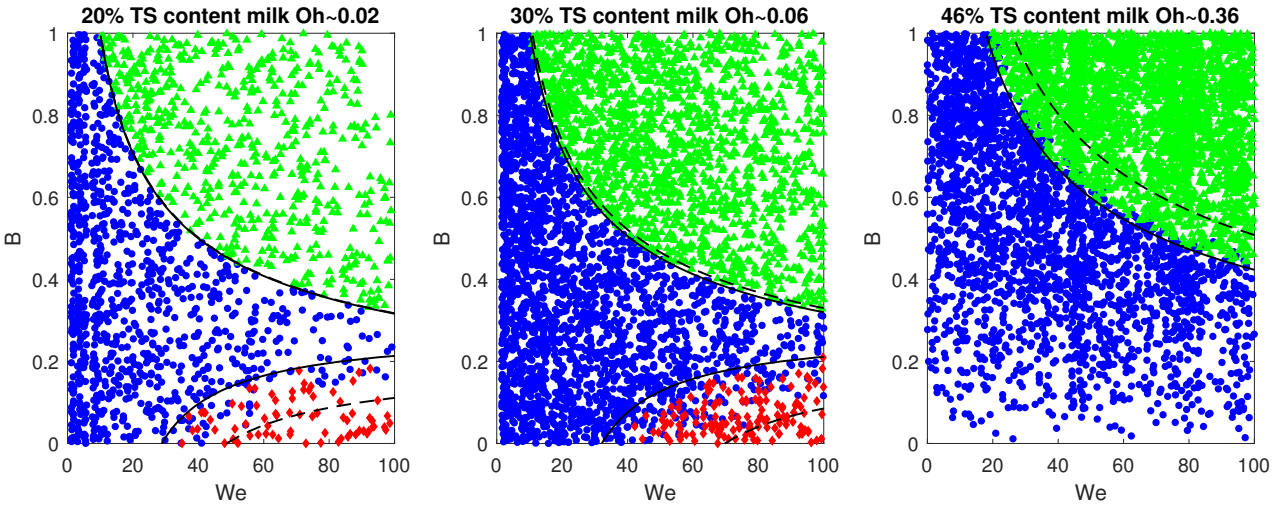


Figure 10: Regime maps of collision outcomes predicted in the current spray model for milk 20%, 30% and 46% TS content. The numerical collisions for reflexive separation are represented in red diamonds, coalescence in blue circles and stretching separation in green triangles. The lines represent the phenomenological model proposed in Finotello et al. [14], with continuous lines for $\Delta$=1 or d=$d_s$ and dashed lines for $\Delta$=0.5 or d=$d_l$.

experimental results with milk concentrates and with $0.5 < \Delta < 1$: reflexive separation (red diamonds), coalescence (blue circles) or stretching separation (green triangles). The lines represent the phenomenological model proposed in Finotello et al. [14]. For the model describing the boundary between coalescence and reflexive separation, the solid lines represent the model for $\Delta$ =1, while the dashed for $\Delta$ =0.5. Note that the coalescence-stretching separation boundary in Finotello et al. [14] is function of the droplet diameter and not of the size ratio. Thus the solid lines of the boundary demarcating coalescence and stretching separation reproduce the model when the smallest droplet, detected during the entire simulation, is considered, while the dashed, when the largest is considered.

### *4.4. Droplet collision outcomes in a spray*

Accounting for the droplet interactions as well as for the dispersion has an effect on the size distribution of the droplets along the spray. It is possible to observe in Fig. 11 that neglecting collisions, the mean Sauter Mean Diameter changes only close to the feed distribution but remains constant in the spray. The SMD is averaged radially only for the locations in presence of droplets. If the collisional interactions are modelled (water without dispersion and with collisions), the SMD tends to increase along the entire axis of the spray. As explained before, the rate of collisions increases if the dispersion model is included leading to a slightly larger SMD (water with collisions and dispersion).

Finotello et al. [14] concluded that the viscosity of the liquid is a very important parameter to predict the collision outcome of a binary droplet collision. The higher viscosity promotes droplet coalescence because the viscous dissipated energy reduces the kinetic energy available to separate the merged droplet. In a spray system it is important to know the distribution of the different types of collisions in the entire system and the prevalence of a certain collision outcome with respect to the others. Moreover it is essential to know the spray characteristics when the viscosity of the liquid is high. For this reason, beside water, we simulate the spray under the same operating conditions but for different liquids: milk 20% TS content,46% TS content and a reference fluid with a very high viscosity, see Tab.2 for the liquid physical properties. Milk 30% TS content is not considered in our analysis because the regime map as well as the collision outcomes occurring in the spray are very similar to milk 20%, thus the general conclusions related to milk 30% are the same as for milk 20%.

In Fig.12 the total number of collisions together with the frequency of collisions over time are shown for the liquids considered in this work. Note that for water, besides coalescence and separation, also bouncing is modelled. For the other liquids, the increase in viscosity reduces the number and the frequencies of collision. Indeed coalescence generates larger drops which are easier to impact again but at the same time reduces the number of droplets available for collision. The collision frequencies in Fig. 12b remain constant over time in the spray already after 0.04 s when the system reaches a steady state. As explained before, the inclusion of turbulent dispersion predicts an enhancement of the collision rates and as a consequences the total number

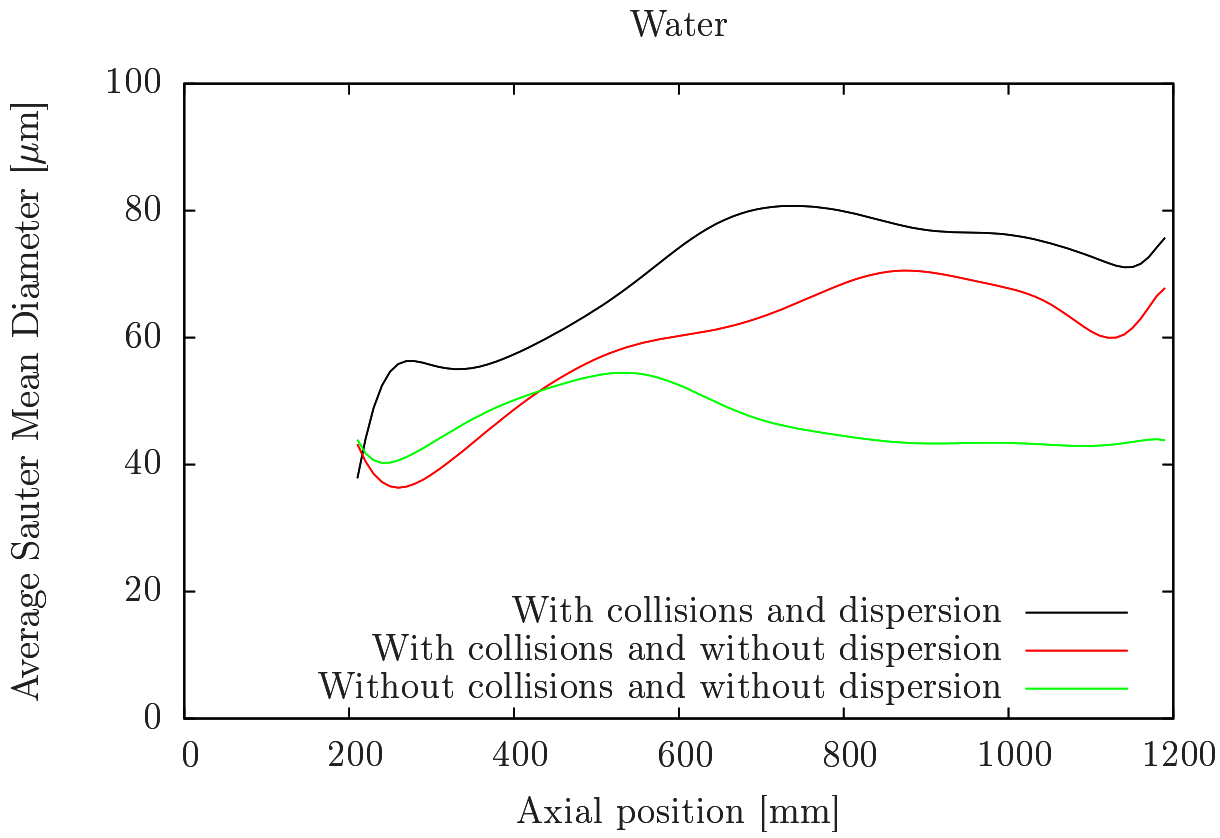


Figure 11: Sauter Mean Diameter averaged in the radial direction as a function of axial position for a water spray in case of presence or absence of collisional interactions and turbulent dispersion model, respectively.

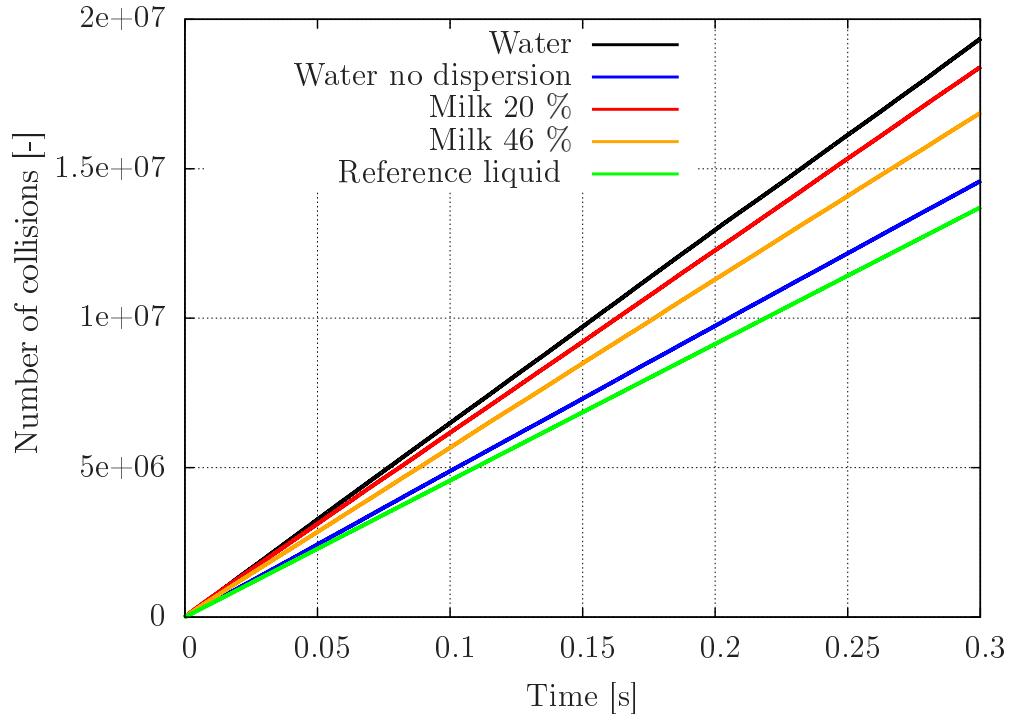


(a)

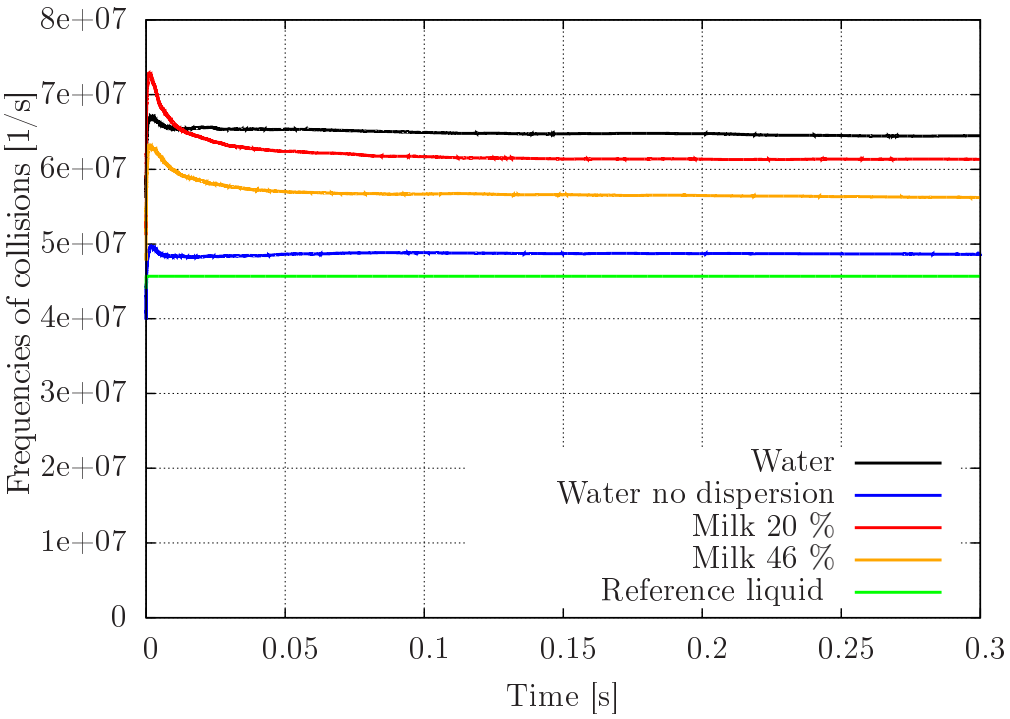


(b)

Figure 12: Total number of collisional events (a) and frequency of collisions (b) for all the liquids considered in this work.

| Liquids | **Coalescence** | **Stretching separation** | **Reflexive separation** | **Bouncing** | **Total number of collisions** ($\cdot 10^6$) |
|---|---|---|---|---|---|
| Water no dispersion | 32.8 % | 34.6 % | 0.3 % | 32.3 % | 14.5 |
| Water | 29.6 % | 34.7 % | 0.5 % | 35.2 % | 19.3 |
| Milk 20% TS | 33.2 % | 66.1 % | 0.7 % | - | 18.3 |
| Milk 46% TS | 36.6 % | 63.3 % | 0.1 % | - | 16.9 |
| Reference fluid | 54.1 % | 45.9 % | - | - | 13.3 |

Table 4: Number of collision outcomes until t=0.3 s for the liquids considered in this work.

of collisions over time.

In Tab. 4 the number of total collisions for the different regimes at t=0.3 s is reported for all the simulations of Fig.12. The turbulence dispersion increases the number of all collisions and in prevalence bouncing and stretching separation. Considering only the viscous liquids the rate of coalescence increases with viscosity while reflexive separation decreases. This is obvious from Fig. 10 where it is observed that the reflexive separation regime is shifted to larger We number. The number of stretching separations increases from water to milk 20% because no bouncing is modelled for milk while decrease from milk 20% to the reference fluid at high viscosity because the boundary between coalescence and separation is shifting to higher We number.

As mentioned before, small droplets follow the turbulent gas velocities while large droplets are uncorrelated with the fluid, and therefore also their relative velocity during collision. In Fig 13 the mean Re and St numbers of the droplets in the entire spray are illustrated together with the total number of coalescence and stretching separation for all the liquids. The profiles of the numerically averaged St number slightly increase in time because of the very large drops generated after coalescence. The Stokes number has larger values for spray of larger viscosity fluids. Note that the viscosity does not directly enter the definition of the Stokes number. Rather, the larger values of the Stokes number can be explained by the fact that for higher viscous liquids the number of coalescence events is larger at the expenses of breakup events, as depicted in

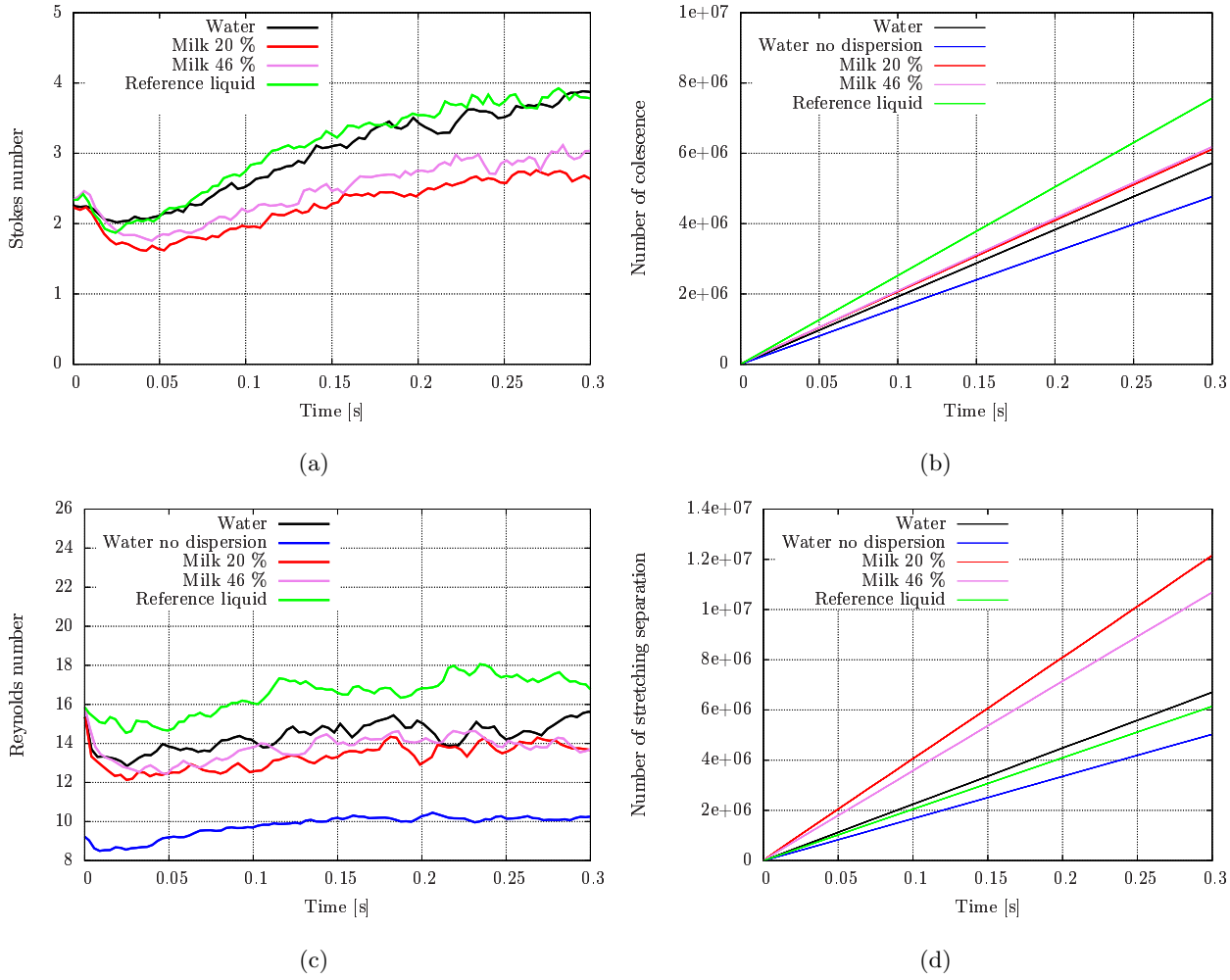


Figure 13: Characterization of the droplets in the entire spray system over time: (a) average Stokes number (b) number of coalescing events (c) average slip-Reynolds number of the droplets and (d) number of stretching separations.

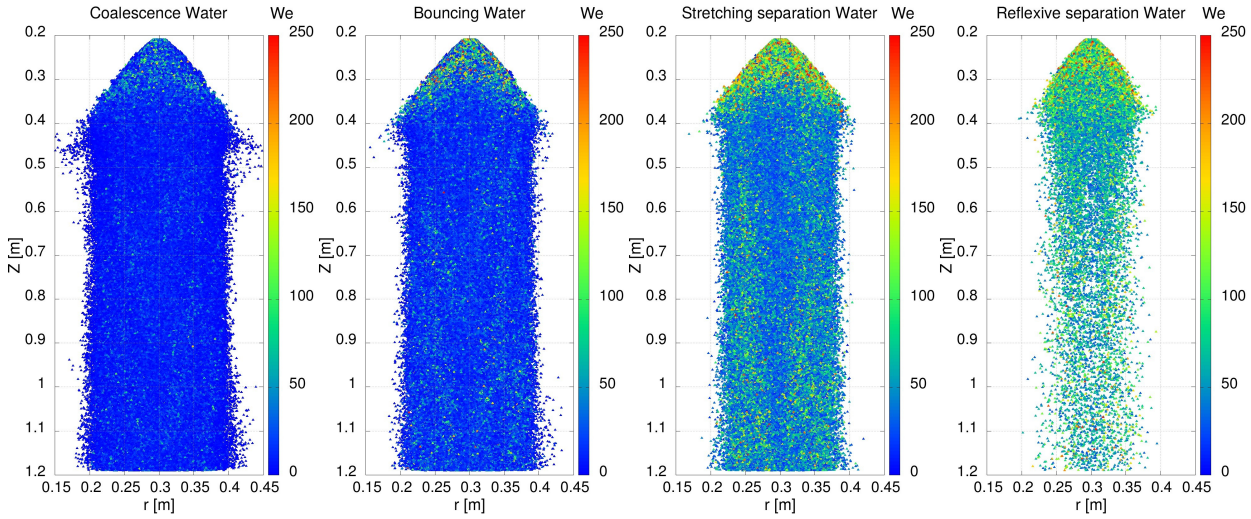


Figure 14: We number of the droplets in the entire spray system for coalescence, bouncing, stretching separation and reflexive separation.)

Fig 13b and Fig. 13d. Larger droplets are rapidly created because of coalescence, which are subsequently less influenced by the gas velocity fluctuations. At the same time we can observe that water has high values of St number relatively to the other liquids and this which is due to the numerous bouncing and coalescence events occurring instead of formation of satellites after separation. For the viscous liquids considered in this work the bouncing regime is replaced mostly by the stretching separation regime and only in a very small extent by coalescence. We decided to report only the number of collisions for stretching separation and not for reflexive separation because the former are more probable and thus significant for the analysis.

The numerically averaged slip-Re number of the droplets in the spray slightly increases with time because of formation of large droplets. As for the St number the relative values of Re numbers between the liquids can be explained by the interplay of coalescence and separation generating satellites of small diameter. Moreover it can be observed that, while the Re number profile for water without dispersion is relatively smooth, the curves with inclusion of turbulence dispersion are oscillating because of subgrid fluctuations.

Apart from the total amount of collisions in the spray it is insightful to know in which areas of the spray we can expect a prevalence of a collision regime with respect to another and what is the spatial evolution of the dimensionless parameters (We, Oh, Re numbers of the droplets) relevant for the droplet-droplet collisions theory. In Fig.14, 15 and 16 these dimensionless numbers are illustrated in the spray of water, separated according to the collision outcome. For example in Fig.14 each marker corresponds to the position

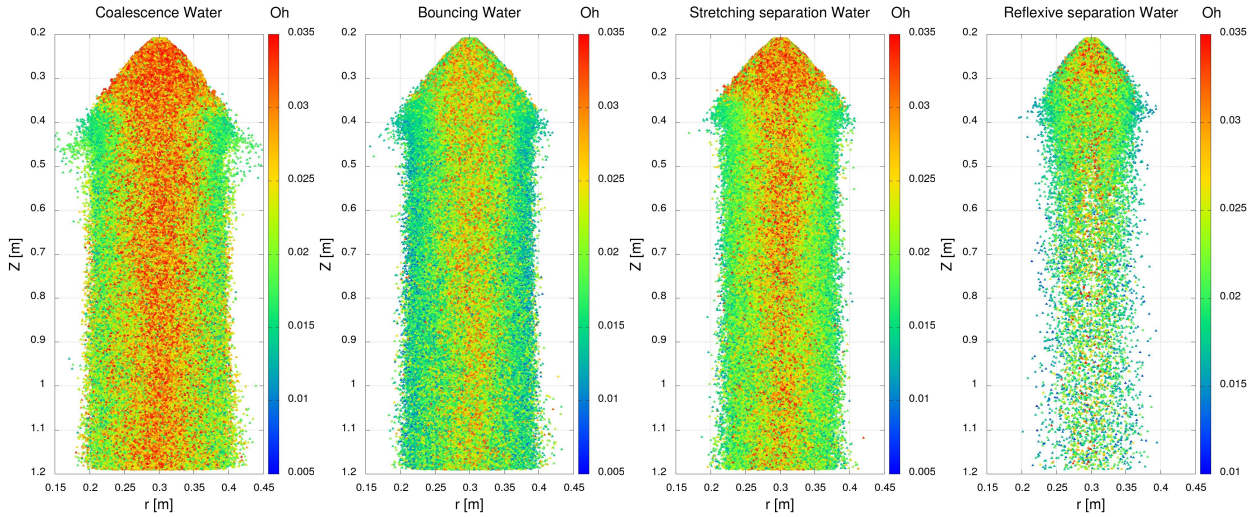


Figure 15: Oh number of the droplets in the entire spray system for coalescence, bouncing, stretching separation and, reflexive separation.

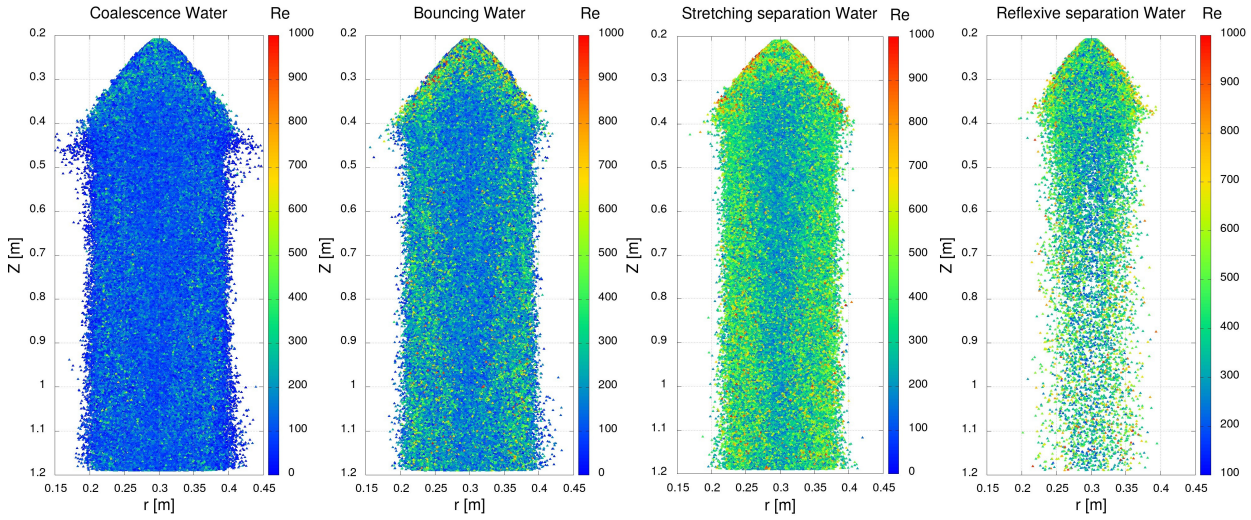


Figure 16: Re number of the droplets in the entire spray system for coalescence, bouncing, stretching separation and, reflexive separation.

in the spray where a pair of droplets coalesced after impact. We decide to show the water profiles because also the dynamics of bounced drops can be compared. Coalescence occurs in a wider volume of the spray while the reflexive separation is limited to the proximity of the symmetry axis where the droplets velocity are higher. Bouncing and stretching separation are distributed in a similar volume of the spray. Another remarkable observation is that the spray width, in which collisions occur, remains straight apart from the initial spray angle were the effect of the radial velocities is larger. In Fig.14 from coalescence to separation the We values increase because the relative velocity necessary for separation is higher than coalescence. In Fig.15 a core region in the spray can be distinguished from the edges of the spray. The Oh number is inversely proportional to the droplet diameter and as a result close to the axis the Oh is higher because the droplet sizes are smaller. The Re number depends also on the relative velocity and the droplet size, therefore the contours in Fig.16 are very similar to the ones for We numbers. Indeed the Re can be expressed as $Re = \sqrt{We}/Oh$.

We warn the reader that the range of We numbers from 0 to 250 in collision regime maps commonly is chosen to clearly show the differences between the collision outcomes contours. We found that actually the droplets in the spray sometimes experience much larger We numbers as illustrated in Fig. 17a for milk 20%. We observe collisions of droplet at very high We number for all the liquids considered in this study. In the initial spray cone, for a length of 20 cm from the inlet of the droplets, the We number for stretching separation reaches up to a We number of 5000. The initial cone of the spray is also the part characterized by the larger rate of collisions. The We numbers remain under 1500 in the straight part of the spray of 1 m length. The scale ranges for the Oh and Re numbers in Fig. 14 are not modified. Moreover we observe that coalescence occurs also at high We number although in the regime map (Fig. 10) this regime ends a bit after We=100. This is the results of a large variation of the droplet size ratio $\Delta$, as depicted in Fig. 17b. These results show that because of the large polydispersity in droplet size, it is important to consider the collision regime maps up to surprisingly large We numbers. Note that at We number of approximately 200 the separation of water droplets is characterized by fingering where the periphery of the expanding disk after impact is wrinkled and formation of very small satellites might occur, Pan et al. [45]. At even larger We number breakup with fragmentation of the disc in satellites and splattering occurs.

Further fundamental research is required to quantify these effects and incorporate the outcome in droplet-unresolved simulations to study large-scale effects in sprays.

## 5. Conclusions

The droplet collision outcomes and their effect on the spray dynamics are studied in an isotherm spray system. A detailed characterization of the collision behaviour inside the spray is beneficial for the design and optimization of spray processes. Knowing the size distribution evolution due to turbulent dispersion

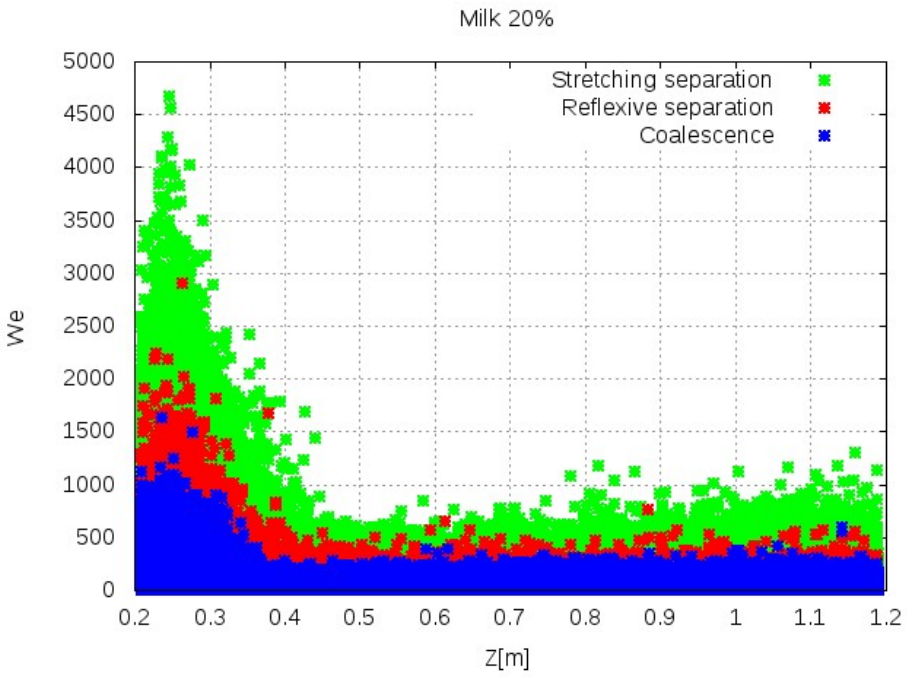


(a)

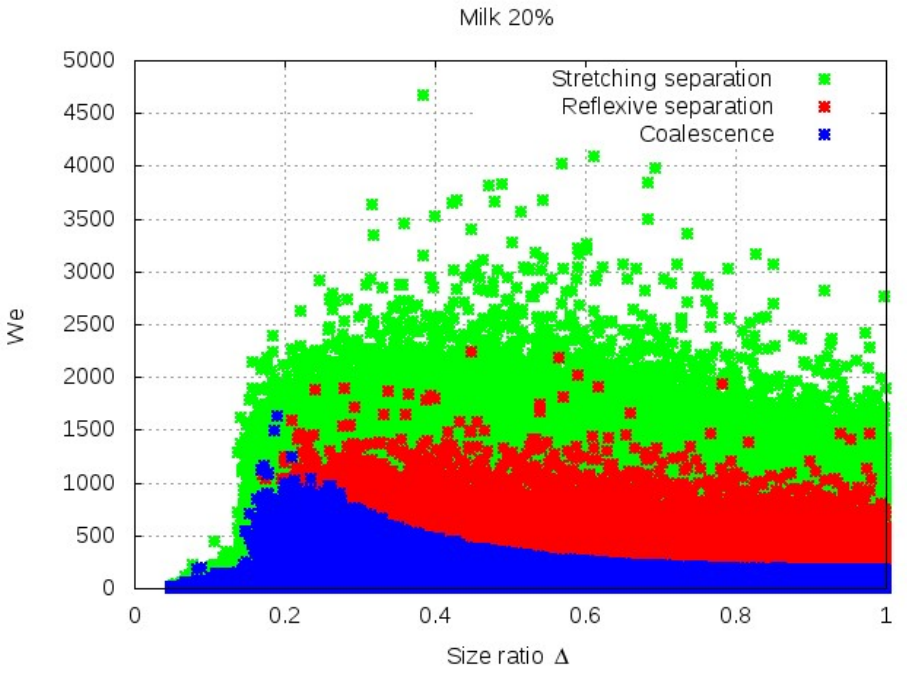


(b)

Figure 17: (a)Distribution of We numbers over the axial position in the spray and (b) distribution of We numbers as a function of the size ratio for collisions of coalescence, stretching and reflexive separation of milk 20%.

and droplet collisions enables us to control parameters such as liquid flow rate, type of atomizer, size of the spray chamber directly to optimize product quality.

The initial atomized distribution evolves along the spray because of the decrease in axial and radial velocities of the droplets which decrease the relative velocity at the moment of impact and, as a consequence, modify the probability of a droplet collision outcomes. In the vicinity of the droplet inlet the breakup events are the most common, producing a large number of very small droplets while at a distance of around 20 cm, for this considered spray, coalescence occurs with formation of larger droplets.

A turbulent dispersion model, based on the Langevin equation, is included to account for stochastic subgrid fluid velocity fluctuations along the droplets trajectory. In general, the turbulent dispersion has the effect of enhancing the collision rates for all regimes without strongly modifying the overall dynamics of the spray in terms of initial spray angle and spray width. This is only strictly valid for the considered spray system and should be checked for other sprays in future work. For our water spray the total number of collisions increases by 25% when including turbulent dispersion. We observe that collisions increase the Sauter Mean Diameter because of coalescence occurring in a wide volume of the spray. This has a strong implication for evaporative processes, where the mechanism of mass and heat transfer between a drop and the fluid medium in which it is moving is influenced by the interface area.

If the viscosity of the liquid is increased, the models for the collision boundaries shift to larger We number with consequent promotion of coalescence. This has a significant effect on the total number of collision in the spray system. Due to coalescence, the number of droplets available to collide decreases, and the collision frequency reduces.

With our work we obtained quantitative data of the collisions for spray of different droplet viscosity and we observed the spatial collision spectra inside the spray. The droplet collisions in the spray are analysed in terms of dimensionless parameters which enables to evaluate the total and local effect of collision outcomes in the spray. This research provides significant new insights in droplet collisions of viscous fluids in a spray where the dispersion due to the turbulent subgrid fluctuations are included. In future work, droplet collisions in the presence of a drying process will be studied.

## Acknowledgement

The work was supported by Tetra Pak CPS, Heerenveen, The Netherlands.

## References

[1] M. Gavaises, A. Theodorakakos, G. Bergeles, G. Brenn, Evaluation of the effect of droplet collisions on spray mixing, Proceedings of the Institution of Mechanical Engineers, Part C: Journal of Mechanical Engineering Science 210 (5) (1996) 465–475.

[2] P. J. O'Rourke, Statistical properties and numerical implementation of a model for droplet dispersion in a turbulent gas, Journal of Computational Physics 83 (2) (1989) 345–360.

[3] M. Ruger, S. Hohmann, M. Sommerfeld, G. Kohnen, Euler/Lagrange calculations of turbulent sprays: the effect of droplet collisions and coalescence, Atomization and sprays 10 (1).

[4] A. Mostafa, H. Mongia, On the modeling of turbulent evaporating sprays: Eulerian versus Lagrangian approach, International Journal of Heat and Mass Transfer 30 (12) (1987) 2583–2593.

[5] J. J. Nijdam, B. Guo, D. F. Fletcher, T. A. Langrish, Lagrangian and Eulerian models for simulating turbulent dispersion and coalescence of droplets within a spray, Applied mathematical modelling 30 (11) (2006) 1196–1211.

[6] A. Gosman, E. Loannides, Aspects of computer simulation of liquid-fueled combustors, Journal of Energy 7 (6) (1983) 482–490.

[7] A. Ormancey, Simulation du comportement de particules dans des écoulements turbulents, Ph.D. thesis, 1984.

[8] R. Perkins, S. Ghosh, J. Phillips, The interaction between particles and coherent structures in a plane turbulent jet, in: Advances in Turbulence 3, Springer, 93–100, 1991.

[9] J. Pozorski, J.-P. Minier, On the Lagrangian turbulent dispersion models based on the Langevin equation, International Journal of Multiphase Flow 24 (6) (1998) 913–945.

[10] M. Breuer, F. Hoppe, Influence of a cost–efficient Langevin subgrid-scale model on the dispersed phase of large–eddy simulations of turbulent bubble–laden and particle–laden flows, International Journal of Multiphase Flow 89 (2017) 23–44.

[11] M. Sommerfeld, Validation of a stochastic Lagrangian modelling approach for inter-particle collisions in homogeneous isotropic turbulence, International Journal of Multiphase Flow 27 (10) (2001) 1829–1858.

[12] N. Ashgriz, J. Poo, Coalescence and separation in binary collisions of liquid drops, Journal of Fluid Mechanics 221 (1990) 183–204.

[13] J.-P. Estrade, H. Carentz, G. Lavergne, Y. Biscos, Experimental investigation of dynamic binary collision of ethanol droplets–a model for droplet coalescence and bouncing, International Journal of Heat and Fluid Flow 20 (5) (1999) 486–491.

[14] G. Finotello, R. F. Kooiman, J. T. Padding, K. A. Buist, A. Jongsma, F. Innings, J. A. M. Kuipers, The dynamics of milk droplet–droplet collisions, Experiments in Fluids 59 (1) (2018) 17.

[15] Y. Jiang, A. Umemura, C. Law, An experimental investigation on the collision behaviour of hydrocarbon droplets, Journal of Fluid Mechanics 234 (1992) 171–190.

[16] J. Qian, C. Law, Regimes of coalescence and separation in droplet collision, Journal of Fluid Mechanics 331 (1997) 59–80.

[17] K. Willis, M. Orme, Experiments on the dynamics of droplet collisions in a vacuum, Experiments in Fluids 29 (4) (2000) 347–358.

[18] K. Willis, M. Orme, Binary droplet collisions in a vacuum environment: an experimental investigation of the role of viscosity, Experiments in fluids 34 (1) (2003) 28–41.

[19] G. Brenn, V. Kolobaric, Satellite droplet formation by unstable binary drop collisions, Physics of Fluids (1994-present) 18 (8) (2006) 087101.

[20] G. Brenn, D. Valkovska, K. Danov, The formation of satellite droplets by unstable binary drop collisions, Physics of Fluids (1994-present) 13 (9) (2001) 2463–2477.

[21] C. Gotaas, P. Havelka, H. A. Jakobsen, H. F. Svendsen, M. Hase, N. Roth, B. Weigand, Effect of viscosity on droplet-droplet collision outcome: Experimental study and numerical comparison, Physics of Fluids (1994-present) 19 (10) (2007) 102106.

[22] O. Kurt, U. Fritsching, G. Schulte, Binary Collisions of Droplets with Fluid and Suspension Particles, ILASS 2007 (2007) 10–12.

[23] M. Kuschel, M. Sommerfeld, Investigation of droplet collisions for solutions with different solids content, Experiments in fluids 54 (2) (2013) 1–17.

[24] M. Sommerfeld, M. Kuschel, Modelling droplet collision outcomes for different substances and viscosities, Experiments in Fluids 57 (12) (2016) 187.

[25] Y. Pan, K. Suga, Numerical simulation of binary liquid droplet collision, Physics of Fluids (1994-present) 17 (8) (2005) 082105.

[26] A. Munnannur, R. D. Reitz, A new predictive model for fragmenting and non-fragmenting binary droplet collisions, International Journal of Multiphase Flow 33 (8) (2007) 873–896.

[27] N. Nikolopoulos, K.-S. Nikas, G. Bergeles, A numerical investigation of central binary collision of droplets, Computers & Fluids 38 (6) (2009) 1191–1202.

[28] C. Focke, D. Bothe, Computational analysis of binary collisions of shear-thinning droplets, Journal of Non-Newtonian Fluid Mechanics 166 (14) (2011) 799–810.

[29] C. Focke, D. Bothe, Direct numerical simulation of binary off-center collisions of shear thinning droplets at high Weber numbers, Physics of Fluids 24 (7) (2012) 59–80.

[30] K. Sun, P. Zhang, C. K. Law, T. Wang, Collision dynamics and internal mixing of droplets of non-Newtonian liquids, Physical Review Applied 4 (5) (2015) 054013.

[31] G. Finotello, S. De, J. C. R. Vrouwenvelder, J. T. Padding, K. A. Buist, A. Jongsma, F. Innings, J. A. M. Kuipers, Experimental investigation of non-Newtonian droplet collisions: the role of extensional viscosity, Experiments in Fluids 59 (7) (2018) 113.

[32] S. K. Pawar, J. T. Padding, N. G. Deen, A. Jongsma, F. Innings, J. A. M. Kuipers, Lagrangian modelling of dilute granular flowmodified stochastic DSMC versus deterministic DPM, Chemical engineering science 105 (2014) 132–142.

[33] S. K. Pawar, J. T. Padding, N. G. Deen, A. Jongsma, F. Innings, J. A. M. Kuipers, Numerical and experimental investigation of induced flow and droplet–droplet interactions in a liquid spray, Chemical Engineering Science 138 (2015) 17–30.

[34] R. Beetstra, M. A. van der Hoef, J. A. M. Kuipers, Drag force of intermediate Reynolds number flow past mono-and bidisperse arrays of spheres, AIChE journal 53 (2) (2007) 489–501.

[35] A. Vreman, An eddy-viscosity subgrid-scale model for turbulent shear flow: Algebraic theory and applications, Physics of Fluids (1994-present) 16 (10) (2004) 3670–3681.

[36] J. Pozorski, S. V. Apte, Filtered particle tracking in isotropic turbulence and stochastic modeling of subgrid-scale dispersion, International Journal of Multiphase Flow 35 (2) (2009) 118–128.

[37] A. Irannejad, F. Jaberi, Large eddy simulation of turbulent spray breakup and evaporation, International Journal of Multiphase Flow 61 (2014) 108–128.

[38] G. A. Bird, Molecular gas dynamics, NASA STI/Recon Technical Report A 76.

[39] M. Du, C. Zhao, B. Zhou, H. Guo, Y. Hao, A modified DSMC method for simulating gas–particle two-phase impinging streams, Chemical Engineering Science 66 (20) (2011) 4922–4931.

[40] Y. Tsuji, T. Tanaka, S. Yonemura, Cluster patterns in circulating fluidized beds predicted by numerical simulation (discrete particle model versus two-fluid model), Powder Technology 95 (3) (1998) 254–264.

[41] H. Hinterbichler, C. Planchette, G. Brenn, Ternary drop collisions, Experiments in fluids 56 (10) (2015) 190.

[42] G. H. Ko, H. S. Ryou, Modeling of droplet collision-induced breakup process, International Journal of Multiphase Flow 31 (6) (2005) 723–738.

[43] J. Madsen, Computational and experimental study of sprays from the breakup of water sheets, Denmark: Aalberg University Esbjerg .

[44] W. T. Coffey, Y. P. Kalmykov, The Langevin equation: with applications to stochastic problems in physics, chemistry

and electrical engineering, vol. 27, World Scientific, 2012.

[45] K.-L. Pan, P.-C. Chou, Y.-J. Tseng, Binary droplet collision at high Weber number, Physical Review E 80 (3) (2009) 036301.